Chapter 4

Transport Modeling

Mark Markofsky · Bernhard Westrich

This section deals with numerical and experimental investigation into the transport behavior of fine reactive sediment fractions interacting with dissolved contaminants in the river environment. The contributions focus on modeling transport processes including sedimentation, erosion, mixing, flocculation, sorption and degradation. In Sect. 4.1, a detailed description of a two-dimensional numerical module for dissolved and particulate contaminant transport in rivers is presented with special emphasis on the interaction of the dissolved and particulate phase and exchange processes between the water column and the uppermost active sediment layer. There is a significant influence of the mixing process at the water-sediment interface on the longitudinal dispersion of a contaminant cloud, caused for example by a flood event. The predictive two-dimensional flow and transport model TELEMAC-SUBIEF/CTM (by EdF) is extended and considered a powerful tool for predicting the dispersion and deposition of hazardous substances disposed after dredging to the fluvial environment. The case study in Sect. 4.2 is an application of the above-mentioned multifractional numerical model for the description of the disposal of highly contaminated dredged material in a regulated river showing the spatial and temporal distribution of the concentration of contaminants in the plume. The results illustrate the trapping effect of the near-bank groyne fields and the river's dead arms, where the contaminant are partly deposited and accumulate. In addition, the numerical investigation also addresses the uncertainty of the model results due to insufficient data about the concentration and fluxes of the considered contaminant. The unsteady flow conditions in the river stretch, the fluctuating input of material by the suction dredger and the interruption of the dredging operation could not be captured sufficiently by the field measurements. Therefore, the model could not be calibrated on data set with high temporal and spatial resolution. A detailed description of a three-dimensional model for calculating the fate of multiple fractions of suspended sediment in an estuarine environment with emphasis on flocculation is given in Sect. 4.3. The counteracting processes of flocculation creating larger floc size and break-up due to turbulent shear forces are described. The sediment is divided into several fractions and the interaction between these fractions is simulated. The numerical model is compared with the coagulation theory and laboratory experiments. A practical application was carried out to find structural measures for the mitigation of sedimentation in a tidal harbor within the Hamburg Harbor system in Germany. It was shown that the model can be used to predict how a current deflection wall can reduce sediment deposition.

Section 4.4 presents a technique for differentiating between various transfer fluxes of fine particles. It is stated that there are serious shortcomings in the modeling options currently available to account consistently for wash-load particle fluxes. The proposed model is based on vortex-drag concepts as an option to predict resistance-to-flow in alluvial streams displaying a dynamic bed morphology evolution. The author considers this a new perspective for simulating the transport of SPM in open channels by acknowledging the role of suction-vortices in actively maintaining the resuspension process. With this concept, the author shows the advantage of significantly lowering the number of model parameters to be calibrated. Application is made to the Scheldt Estuarine System by Antwerp.

George K. Jacoub · Bernhard Westrich

4.1 Two-Dimensional Numerical Module for Contaminant Transport in Rivers

4.1.1 Introduction

Contaminants such as heavy metals or organic pollutants are adsorbed to fine sediment particles which are transported through the river system and deposited in the regions of low flow velocities. This results in potential sources of contaminants called "hot spots" which can be eroded by floods causing deterioration of the river water quality. Therefore, the erosion, transport and deposition of contaminated sediments play a significant role in water resources engineering and management. It is a challenging task to model and predict the pathway and fate of contaminated sediments with emphasis on their spatial and temporal distribution in surface waters.

There has been intensive research trying to address the contaminant transport in river systems based on assumptions and simplifications according to each study case. This study however, presents the development of a 2-D numerical module which deals with an entire physical concept of contaminant transport in rivers. The development is based on the TELEMAC-System which consists of several modules (EDF 2002). One of them is TELEMAC-2D which solves the classical hydrodynamic Saint-Venant equations and the other one is SUBIEF-2D which handles the suspended sediment transport. Both modules are programmed in Fortran 90 and based on the Finite Element formulations with unstructured grid. The new developments are focused on the SUBIEF-2D module and named as CTM-SUBIEF-2D which stands for Contaminant Transport Module-SUBIEF-2D. The CTM-SUBIEF-2D module describes the transport of dissolved and adsorbed substances in the water column and the river bed with emphasis on the interaction between dissolved and adsorbed contaminants using the first order sorption kinetics "k_d concept". Physical processes such as sedimentation, erosion, diffusion and degradation are taken into account. The physical based model concept and the numerical implementation of the new developments are presented in the following sections.

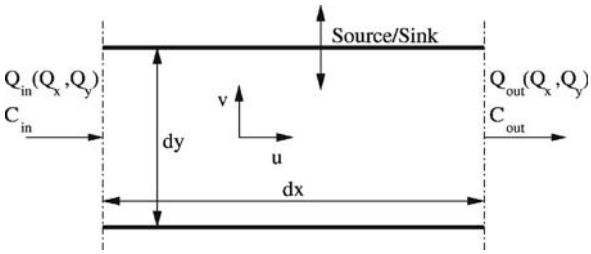

Fig. 4.1.
Illustration of two dimensions inflow/outflow of discharge and concentration

4.1.2 Module Concept and Assumption

The numerical code used in this study is the TELEMAC-System code which consists of several modules. One of them is the transport module, SUBIEF-2D, which deals with the transport of one or several tracers in a two-dimensional free surface flow. SUBEF-2D has been designed on the basis of the finite element method and the results are integrated over the water depth according to Eq. 4.1 and the concept of the mass balance of a solute which is derived for a river section (horizontal plane) with a length of dx and a width of dy as shown in Fig. 4.1.

The mass conservation equation is written in terms of a depth averaged concentration and consists of local derivative, advection, diffusion and source or sink terms as defined in Eq. 4.1.

$$\frac{\partial C}{\partial t} + u\frac{\partial C}{\partial x} + v\frac{\partial C}{\partial y} = \underline{\underline{D}}\left[\frac{\partial^2 C}{\partial x^2} + \frac{\partial^2 C}{\partial y^2}\right] + \frac{S_o}{\bar{h}} \tag{4.1}$$

in which C is the substance mass per unit volume (kg m^{-3}), t is the time (s), u and v are the depth averaged velocity components in x,y-directions (m s^{-1}), $\underline{\underline{D}}$ is the dispersion tensor (m^2 s^{-1}), S_o is the source or sink (kg m^{-2} s^{-1}) and $\bar{h}$ is the average water depth (m).

As contaminant transport modeling in river systems represents a great challenge to numerically model and predict the fate of contaminated sediments in fluvial systems, a two-dimensional contaminant transport module has been developed based on SUBIEF-2D module. The developed module, CTM-SUBIEF-2D, deals with the mass conservation for five variables as shown in (Fig. 4.2): suspended sediment (SS), dissolved contaminant (C_D) and adsorbed contaminant (C_A) in the water column as well as in the river bed (G_D and G_A). The partitioning between the two variables is described by a kinetic sorption mechanism of first order in both the water column and the pore water of a river bed (Chapra 1997). The exchange between the river bed and the water column for the dissolved contaminants is driven by the concentration gradient in the water/sediment interface in a diffusive manner and for the adsorbed contaminants the exchange is controlled by sedimentation and erosion processes. The diffusion coefficient, D_S, is taken constant both in space and time and can be determined according to the experimental studies of Haag 2003. During the transport, contaminants are subject to degradation. In this research, a first-order decay is assumed for all chemical and biological reactions, i.e. the rate loss of contaminants is proportional to the concentration at any time, and it can be defined as, $-\lambda_d C$, (Thomann and Mueller 1987 and James 1993).

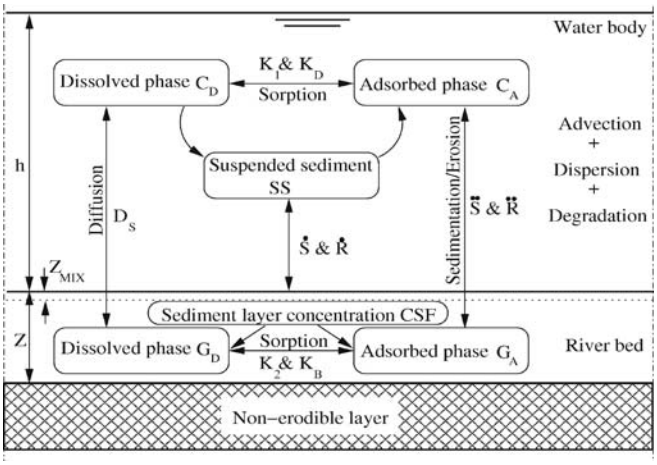

Fig. 4.2.
Physical concept of the developed module CTM-SUBIEF-2D

The transport governing equations of the five variables can be given in the form of:

1. Mass conservation for suspended sediment in the water column, SS:

$$\frac{\partial \mathrm{SS}}{\partial t} + \underline{u}\,\mathrm{grad}\,\mathrm{SS} = div\left(\underline{\underline{D}}\,\mathrm{grad}\,\mathrm{SS}\right) - \frac{S^{\bullet} - R^{\bullet}}{\bar{h}} + S_{\mathrm{SS}}$$
$$\text{where} \quad S^{\bullet} = V_{\mathrm{S}}\mathrm{SS}\left[1 - \frac{\tau_{\mathrm{b}}}{\tau_{\mathrm{cd}}}\right], \quad R^{\bullet} = M\left[\frac{\tau_{\mathrm{b}}}{\tau_{\mathrm{ce}}} - 1\right] \tag{4.2}$$

2. Mass conservation for the dissolved contaminant in the water column, C_{D}:

$$\frac{\partial C_{\mathrm{D}}}{\partial t} + \underline{u}\,\mathrm{grad}C_{\mathrm{D}} = div\left(\underline{\underline{D}}\,\mathrm{grad}C_{\mathrm{D}}\right) - K_1\left(K_{\mathrm{D}}\mathrm{SS}C_{\mathrm{D}} - C_{\mathrm{A}}\right) - \frac{D_{\mathrm{S}}}{Z_{\mathrm{AB}}}\frac{\left(C_{\mathrm{D}} - G_{\mathrm{D}}\right)}{\bar{h}} - \lambda_{\mathrm{d}}C_{\mathrm{D}} + S_{\mathrm{CD}} \tag{4.3}$$

3. Mass conservation for the adsorbed contaminant in the water column, C_{A}:

$$\frac{\partial C_{\mathrm{A}}}{\partial t} + \underline{u}\,\mathrm{grad}C_{\mathrm{A}} = div\left(\underline{\underline{D}}\,\mathrm{grad}C_{\mathrm{A}}\right) + K_1\left(K_{\mathrm{D}}\mathrm{SS}C_{\mathrm{D}} - C_{\mathrm{A}}\right) - \frac{S^{\bullet\bullet} - R^{\bullet\bullet}}{\bar{h}} - \lambda_{\mathrm{d}}C_{\mathrm{A}} + S_{\mathrm{CA}} \tag{4.4}$$

4. Mass conservation for the dissolved contaminant in the river bed (pores media), G_{D}:

$$\frac{\partial G_{\mathrm{D}}}{\partial t} = \frac{D_{\mathrm{S}}}{Z_{\mathrm{AB}}}\frac{\left(C_{\mathrm{D}} - G_{\mathrm{D}}\right)}{Z_{\mathrm{MIX}}} - K_2\left(K_{\mathrm{B}}\mathrm{CSF}G_{\mathrm{D}} - G_{\mathrm{A}}\right) - \lambda_{\mathrm{d}}G_{\mathrm{D}} \tag{4.5}$$

5. Mass conservation for the adsorbed contaminant in the river bed (sediments), G_A:

$$\frac{\partial G_A}{\partial t} = K_2\left(K_B \mathrm{CSF} G_D - G_A\right) + \frac{S^{\bullet\bullet} - R^{\bullet\bullet}}{Z_{MIX}} - \lambda_d G_A$$
$$\text{where} \quad S^{\bullet\bullet} = \frac{C_A}{SS} S^{\bullet} \quad , \quad R^{\bullet\bullet} = \frac{G_A}{CSF} R^{\bullet} \tag{4.6}$$

in which $S^{\bullet}$, $R^{\bullet}$, $S^{\bullet\bullet}$ and $R^{\bullet\bullet}$ are the sedimentation and erosion rates for the suspended sediment and adsorbed contaminant in both the water body and the river bed (kg m^{-2} s^{-1}), τ_b is the bed shear stress (N m^{-2}), τ_{cd} is the critical bed shear stress at which deposition begins (N m^{-2}), τ_{ce} is the critical bed shear stress for erosion (N m^{-2}), V_S is the fall velocity of suspended sediments (m s^{-1}), M is erosion coefficient (kg m^{-2} s^{-1}), Z_{AB} is the attributed thickness where the diffusion takes places into the water/sediment interface at the river bed (m), D_S is the diffusion coefficient to the river bed (m^2 s^{-1}), Z_{MIX} is the mixing layer thickness (m), λ_d is the specific decay constant coefficient (s^{-1}), K_1 is the sorption kinetics in the water body (s^{-1}), K_2 is the sorption kinetics in the river bed (s^{-1}), K_D is the equilibrium sorption coefficient in the water body (m^3 kg^{-1}), K_B is the equilibrium sorption coefficient in the river bed (m^3 kg^{-1}), CSF is the deposited or eroded sediment layer concentration (kg m^{-3}), S_{SS}, S_{CD} and S_{CA} are the source/sink terms for the suspended sediment, dissolved and adsorbed contaminants in the water body respectively, $\underline{D}$ is dispersion tensor (m^2 s^{-1}) and $\bar{h}$ is the average water depth (m).

In the CTM-SUBIEF-2D module, a single active sediment layer of thickness Z is considered where sedimentation, erosion and mixing take place. This concept of having a single layer is supported as an option for reasonable results as long as short term simulations are performed (Di Silvio 1991 and Sieben 1996). If only sedimentation of pure and contaminated sediments occurs, then the concentration of contaminants is averagely integrated over the deposited layer thickness ΔZ. If the active layer Z is contaminated and erosion occurs, the concentration of contaminant rest is determined over the thickness $Z - \Delta Z$, Fig. 4.3.

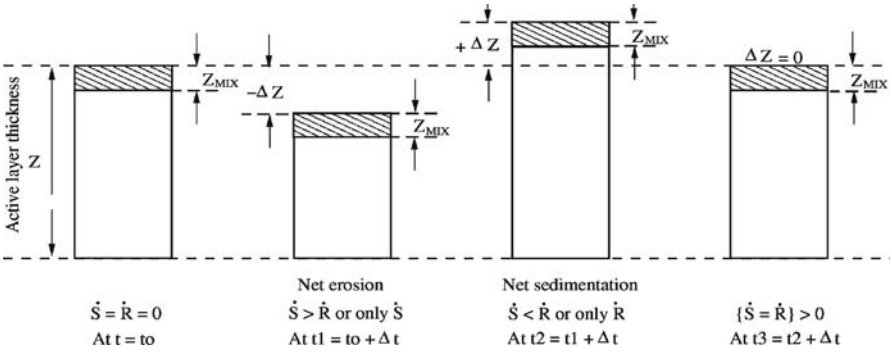

Fig. 4.3. Simplified concept of the mixing layer used in the developed module CTM-SUBIEF-2D

Mixing becomes more important and dominates the river bed contaminant concentrations if sedimentation and erosion take place simultaneously at about the same rate. The mixing process is assumed to occur at a very thin top layer of deposited sediments. In general, the thickness of this layer, Z_{MIX}, is a key parameter depending on bed shear intensity and sediment properties which change in space and time. It is difficult to determine or measure this thickness because of lack of data. The Z_{MIX} thickness should be neither too thin so that it remains the same during one numerical time-step simulation nor too large in order to reproduce effective changes of the bed composition during the simulation (Belleudy and Sogreah 2000 and 2001). Therefore, it is assumed that the minimum thickness should equal the smallest sediment fraction in order to allow mixing.

The exchange rates between the dissolved and adsorbed contaminants in both the water body and the river bed are controlled by sorption processes. These processes can be mathematically presented in terms of equilibrium distribution coefficients and sorption kinetics which are calculated considering steady-state hydraulic conditions and defined as (Santschi and Honeyman 1989 and Carrol and Harms 1999):

$$\mathrm{SSK_D} = \lim_{t\to\infty}\left[\frac{C_A}{C_D}\right] \quad \text{and} \quad \mathrm{CSFK_B} = \lim_{t\to\infty}\left[\frac{G_A}{G_D}\right] \tag{4.7}$$

In the Eqs. 4.5 and 4.6, the dissolved and adsorbed concentrations are calculated from the mass rate of contaminants deposited or eroded. The right hand side of these equations is obtained as follows:

$$\begin{aligned}\frac{\partial m_D}{\partial t} &= \frac{\partial\left(G_D Z_{MIX}\right)}{\partial t} = Z_{MIX}\frac{\partial G_D}{\partial t} + G_D\frac{\partial Z_{MIX}}{\partial t}\\ \frac{\partial m_A}{\partial t} &= \frac{\partial\left(G_A Z_{MIX}\right)}{\partial t} = Z_{MIX}\frac{\partial G_A}{\partial t} + G_A\frac{\partial Z_{MIX}}{\partial t}\end{aligned} \tag{4.8}$$

Assuming that the Z_{MIX} is independent of time, which is acceptable when short term simulations are performed, then the Eq. 4.8 can be rewritten as:

$$\frac{\partial m_D}{\partial t} = Z_{MIX}\frac{\partial G_D}{\partial t} \quad \text{and} \quad \frac{\partial m_A}{\partial t} = Z_{MIX}\frac{\partial G_A}{\partial t} \tag{4.9}$$

in which m_D and m_A are the dissolved and adsorbed masses per unit area of river bed in pores media and sediments, respectively (kg m^{-2}).

In the Eqs. 4.5 and 4.6, the advection terms do not appear because the advective transport velocity in the river bed is negligible when compared to the flow velocity in the water column. Therefore, the module accounts for the vertical exchange of contaminants between the water column and the river bed. Then, these equations are treated using the Finite Difference method.

4.1.3 Numerical Implementation

The governing equations of the CTM-SUBIEF-2D module are characterized by the advection-diffusion terms and hence, they are classified as parabolic-hyperbolic equations. Two numerical methods have been implemented to treat the transport equations as follows:

1. The method of operator splitting.
2. The method of Streamline Upwind Petrov-Galerkin "SUPG".

Operator Splitting Method

The solution of the transport equation procedure has two steps, e.g., an advection step (first step) and a diffusive step (second step) as shown in Eq. 4.10.

$$\frac{\partial C}{\partial t} \approx \frac{\Delta C}{\Delta t} = \underbrace{\frac{\tilde{C} - C^n}{\Delta t}}_{\text{First step}} + \underbrace{\frac{C^{n+1} - \tilde{C}}{\Delta t}}_{\text{Second step}} \tag{4.10}$$

in which C is the substance concentration (kg m^{-3}), $\tilde{C}$ is the pre-solution concentration of C (kg m^{-3}), C^n and C^{n+1} are the concentration of C at $t = n$ and $t = n + 1$, respectively (kg m^{-3}).

In the first step, the advection term is treated by the method of characteristics "MOC" using the Runge-Kutta scheme of the first order and the interpolation of characteristics within the elements conforms to the finite elements method. According to the principles of Runge-Kutta scheme and assuming that the velocity vector at a node of an element is constant during the time step, the characteristics of each variable can be determined as follows:

$$\begin{aligned}
&\frac{\tilde{\mathrm{SS}} - \mathrm{SS}^n}{\Delta t} + \underline{u}\,\mathrm{grad}\,\mathrm{SS} = 0 \quad \Leftrightarrow \quad \frac{\mathrm{dSS}}{\mathrm{d}t} = 0 \\
&\frac{\tilde{C}_\mathrm{D} - C_\mathrm{D}^n}{\Delta t} + \underline{u}\,\mathrm{grad}\,C_\mathrm{D} = 0 \quad \Leftrightarrow \quad \frac{\mathrm{d}C_\mathrm{D}}{\mathrm{d}t} = 0 \\
&\frac{\tilde{C}_\mathrm{A} - C_\mathrm{A}^n}{\Delta t} + \underline{u}\,\mathrm{grad}\,C_\mathrm{A} = 0 \quad \Leftrightarrow \quad \frac{\mathrm{d}C_\mathrm{A}}{\mathrm{d}t} = 0
\end{aligned} \tag{4.11}$$

In the second step, Finite Difference and Finite Element methods are used for time and space discretizations, respectively. In the finite difference method, the concentration C at time step $n + 1$ is calculated from Eq. 4.12 where $\tilde{C}$ is obtained from the advection step (first step). The unknown concentration C on the right hand side of Eq. 4.12 can be replaced by the Eq. 4.13.

$$\frac{C^{n+1} - \tilde{C}}{\Delta t} = div\left(\underline{\underline{D}}\,\mathrm{grad}\,C\right) + \mathrm{Source/Sink} + \mathrm{other\ terms} \tag{4.12}$$

$$C = \theta C^{n+1} + (1-\theta)C^n \tag{4.13}$$

in which θ is the implicit parameter varying from 0 (fully explicit) to 1 (fully implicit). It is recommended to use θ between 0.5 and 0.6 for good and stable results. If θ is between 0 and 0.5, then the stability of the results is not ensured (Hinkelmann 2002).

Other spatial terms of the transport equation can be treated with the Finite Element method. The concentration variable C can be replaced by an approximated value C resulting from summing up the products of interpolation functions N_i and the node value C_i as shown in Eq. 4.14:

$$C^n = \widehat{C}^n = \sum_{i=1}^{i=3} N_i \widehat{C}_i^n = N_1\widehat{C}_1^n + N_2\widehat{C}_2^n + N_3\widehat{C}_3^n \tag{4.14}$$

in which i is the number of nodes per element. Three nodes per element are commonly used in the TELEMAC-System.

When Eq. 4.14 is substituted into Eqs. 4.2–4.4 (setting up all terms on the right side), they do not equal to zero any longer but have a residual error ε, Eq. 4.15. In order to eliminate this error, the method of weighted residuals is used which can be applied by multiplying the residual error by a weighting function N_j and integrating this quantity over the computational domain Ω, Eq. 4.15.

$$\frac{\partial \widehat{C}}{\partial t} - \underline{\underline{D}}\frac{\partial^2 \widehat{C}}{\partial x^2} - \underline{\underline{D}}\frac{\partial^2 \widehat{C}}{\partial y^2} - \text{Source/Sink} = \varepsilon \quad , \quad \int_\Omega N_j \varepsilon \mathrm{d}\Omega = 0 \tag{4.15}$$

Using the Standard-Galerkin method, the $N_j = N_i$, the following form can be obtained:

$$\int_\Omega N_j \left(\frac{\partial \widehat{C}}{\partial t} - \underline{\underline{D}}\frac{\partial^2 \widehat{C}}{\partial x^2} - \underline{\underline{D}}\frac{\partial^2 \widehat{C}}{\partial y^2} - \text{Source/Sink} \right) \mathrm{d}\Omega = 0 \tag{4.16}$$

Equation 4.16 includes turbulent diffusion and source/sink terms that can be treated using the Green-Gauss theory according to the form:

$$\int_\Omega div(\alpha \underline{v}) \mathrm{d}\Omega = \int_\Omega \alpha \, div\, \underline{v} \mathrm{d}\Omega + \int_\Omega \mathrm{grad}\, \alpha \underline{v} \mathrm{d}\Omega = \int_\Gamma (\alpha \underline{v}) \underline{n} \mathrm{d}\Gamma \tag{4.17}$$

in which Γ is the boundary of the computation domain, α is a scalar value, $\underline{v}$ is a vector and $\underline{n}$ is the norm vector perpendicular on the boundary line.

Applying this concept to the transport equation and assuming that $\alpha = N_j$ and $\underline{v} = \mathrm{grad}\, \widehat{C}$, the following equation can be obtained:

$$-\int_\Omega N_j div\left(\underline{\underline{D}}\, \mathrm{grad}\, \widehat{C}\right) \mathrm{d}\Omega = \underbrace{-\int_\Gamma N_j \underline{\underline{D}}\, \mathrm{grad}\, \widehat{C} \mathrm{d}\Gamma}_{=\text{zero}} + \int_\Gamma \mathrm{grad}\, N_j \underline{\underline{D}}\, \mathrm{grad}\, \widehat{C} \mathrm{d}\Omega$$
$$\mathrm{grad}\widehat{C} = \left[\theta \widehat{C}^{n+1} + (1-\theta)\widehat{C}^n\right] \tag{4.18}$$

The integration over the boundary of the computational domain is zero which is represented by the first term of the right side of the Eq. 4.18. Applying this equation to the transport equations, the following set of terms of the transport equation is obtained as:

$$
\begin{aligned}
\text{Temporal term} &= \frac{\widehat{C}^{n+1} - \widehat{C}^{\text{advection}}}{\Delta t} \underbrace{\int_{\Omega} N_i N_j \mathrm{d}\Omega}_{\text{Mass Matrix}} \\
\text{Dispersion term} &= \left[\theta \widehat{C}^{n+1} + (1-\theta)\widehat{C}^{n}\right] \underbrace{\int_{\Omega} \operatorname{grad} N_j \underline{\underline{D}} \operatorname{grad} N_i \mathrm{d}\Omega}_{\text{Dispersion Matrix}} \\
\text{Sorption term} &= -\left[\theta \widehat{C}_{\mathrm{D}}^{n+1} + (1-\theta)\widehat{C}_{\mathrm{D}}^{n}\right] K_1 K_{\mathrm{D}} \mathrm{SS} \underbrace{\int_{\Omega} N_i N_j \mathrm{d}\Omega}_{\text{Mass Matrix}} \\
&\quad + \left[\theta \widehat{C}_{\mathrm{A}}^{n+1} + (1-\theta)\widehat{C}_{\mathrm{A}}^{n}\right] K_1 \underbrace{\int_{\Omega} N_i N_j \mathrm{d}\Omega}_{\text{Mass Matrix}} \\
\text{Degradation term} &= \left[\theta \widehat{C}_{\mathrm{D}}^{n+1} + (1-\theta)\widehat{C}_{\mathrm{D}}^{n}\right] \lambda_{\mathrm{d}} \underbrace{\int_{\Omega} N_i N_j \mathrm{d}\Omega}_{\text{Mass Matrix}} \\
\text{Source/Sink term} &= S_{\mathrm{o}} \underbrace{\int_{\Omega} N_i N_j \mathrm{d}\Omega}_{\text{Mass Matrix}}
\end{aligned}
\tag{4.19}
$$

in which C represents the concentrations of suspended sediment (SS), dissolved contaminant (C_{D}) and adsorbed contaminant (C_{A}).

There is a great number of references in literature which handle the treatment and the implementation of the mass and dispersion matrixes of Eq. 4.19. These matrixes have already been numerically treated in the TELEMAC-System (EDF 2002). The following steps are carried out to rearrange and implement the transport equations:

1. applying the procedure mentioned in Eq. 4.19 to the five transport equations;
2. replacing $\mathrm{d}\Omega$ by $\mathrm{d}x\mathrm{d}y$ for a two dimensions model;
3. setting the unknown variables on the left-hand side of the equations and all known variables with coupling terms on the right-hand side;
4. using the Jacobi matrix to transform the derivatives of the interpolation functions after considering the Cartesian coordinates.

Herewith, a representative rearranged transport equation of the adsorbed contaminant in the water column, C_{A}, is shown in Eq. 4.20. The other transport equations of SS and C_{D} have the same structure.

$$
\begin{aligned}
&C_{\mathrm{A}}^{n+1}\left(\left[\frac{1}{\Delta t}+\theta K_1+\theta\lambda_{\mathrm{d}}\right]\iint\limits_{x,y} N_i N_j \mathrm{d}x\mathrm{d}y\right)-\theta C_{\mathrm{A}}^{n+1}\iint\limits_{x,y}\operatorname{grad} N_j \underline{\underline{D}}\operatorname{grad} N_i \mathrm{d}x\mathrm{d}y\\
&=\left(\begin{array}{l}\left[\dfrac{\tilde{C}_{\mathrm{A}}^{\mathrm{advection}}}{\Delta t}-(1-\theta)K_1\Delta t C_{\mathrm{A}}^{n}+\underline{\underline{\theta K_1 K_{\mathrm{D}}\Delta t \mathrm{SSC}_{\mathrm{D}}^{n+1}}}+(1-\theta)K_1K_{\mathrm{D}}\Delta t\mathrm{SSC}_{\mathrm{D}}^{n}-\right.\\ \left.(1-\theta)\lambda_{\mathrm{d}}+\ddot{R}-\ddot{S}\pm S_{\mathrm{o}}\right]\\ \iint\limits_{x,y} N_i N_j \mathrm{d}x\mathrm{d}y\end{array}\right)\\
&+(1-\theta)C_{\mathrm{A}}^{n}\iint\limits_{x,y}\operatorname{grad} N_j \underline{\underline{D}}\operatorname{grad} N_i dxdy
\end{aligned}
\tag{4.20}
$$

According to the section above, the transport equation of dissolved and adsorbed contaminants in the river bed (G_{D} and G_{A}, respectively) are determined from:

$$
\begin{aligned}
&G_{\mathrm{D}}^{n+1}\left[1+\theta\frac{D_{\mathrm{S}}}{Z_{\mathrm{MIX}}Z_{\mathrm{AB}}}\Delta t+\theta K_2K_{\mathrm{B}}\Delta t\right]\\
&=G_{\mathrm{D}}^{n}\left[1-(1-\theta)\frac{D_{\mathrm{S}}}{Z_{\mathrm{MIX}}Z_{\mathrm{AB}}}\Delta t-(1-\theta)K_2K_{\mathrm{B}}\Delta t\right]\\
&\quad+\frac{D_{\mathrm{S}}}{Z_{\mathrm{MIX}}Z_{\mathrm{AB}}}\Delta t\left[\theta C_{\mathrm{D}}^{n+1}+(1-\theta)C_{\mathrm{D}}^{n}\right]+K_2\Delta t\left[\underline{\underline{\theta G_{\mathrm{A}}^{n+1}}}+(1-\theta)G_{\mathrm{A}}^{n}\right]\quad\text{and,}
\end{aligned}
\tag{4.21}
$$

$$
\begin{aligned}
G_{\mathrm{A}}^{n+1}\left[1+\theta K_2\Delta t\right]&=G_{\mathrm{A}}^{n}\left[1-(1-\theta)K_2\Delta t\right]+K_2\Delta t\left[\underline{\underline{\theta K_{\mathrm{B}}G_{\mathrm{D}}^{n+1}}}+(1-\theta)K_{\mathrm{B}}G_{\mathrm{D}}^{n}\right]\\
&\quad+\left[\frac{S^{\bullet\bullet}-R^{\bullet\bullet}}{Z_{\mathrm{MIX}}}\right]\Delta t
\end{aligned}
\tag{4.22}
$$

Streamline Upwind/Petrov-Galerkin "SUPG"

The method focuses on how to treat the advection term using the central difference and optimal upwind scheme. The last is developed on the basis of an artificial diffusion $\tilde{k}$ (Kelly et al. 1980). The scalar value of the artificial diffusion can be calculated from Eq. 4.23 as it is implemented in the TELEMAC-System.

$$
\begin{aligned}
&\tilde{k}=\frac{\delta\Delta X}{2}\quad,\quad\text{where}\\
&\delta=0\ \Rightarrow\ \text{Normal central scheme}\\
&\delta=1\ \Rightarrow\ \text{Upwind/Petrov}-\text{Galerkin scheme}\\
&\delta=C_{\mathrm{r}}
\end{aligned}
\tag{4.23}
$$

in which δ is the upwind scheme coefficient (–), Cr is the Courant number = $(u\Delta t)/(\Delta X)$, Δt is the time step (s) and ΔX is the grid distance of the element (m).

If the Standard Galerkin Weighted Residual method is used, the weighting function is considered to be continuous across inter-boundaries but it may have discontinuity at the elements nodes. The SUPG method formulation considers this effect and requires a discontinuous weighting function as shown below:

$$\varpi = \omega + p \tag{4.24}$$

in which ϖ is the weighting function according to the SUPG, ω is the continuous weighting function and p is the discontinuous weighting function of lower degree (Brooks and Huges 1982).

They found that the p function equals to the upwind artificial diffusion tensor $\tilde{k}_{ij}$ with some modifications to consider the effect of the local mean velocity at each node u.

$$\varpi = \omega + \frac{\tilde{k}_{ij} u_j \underline{\omega}}{\|u\|} \tag{4.25}$$

in which $\underline{\omega}$ is a certain function that depends on the advection term.

The weighting function $\underline{\omega}$ has to be applied to all terms of the transport equation. However, Brooks and Huges 1982 have shown that the method SUPG can not be used to treat the diffusion and the source/sink terms. Those terms can be then treated using the finite element method as mentioned above. After applying the SUPG basic functions as explained above to only the advection term in the transport equations, the following is obtained:

$$\begin{aligned}
&\int_\Omega \frac{\tilde{\mathrm{SS}} - \mathrm{SS}^n}{\Delta t} \mathrm{d}\Omega + \int_\Omega \omega \underline{u} \,\mathrm{grad}\,\mathrm{SS} \mathrm{d}\Omega + \int_\Omega \frac{\tilde{k}_{ij} u_j \underline{\omega}}{\|u\|} \underline{u} \,\mathrm{grad}\,\mathrm{SS} \mathrm{d}\Omega = 0 \\
&\int_\Omega \frac{\tilde{C}_\mathrm{D} - C_\mathrm{D}^\mathrm{n}}{\Delta t} \mathrm{d}\Omega + \int_\Omega \omega \underline{u} \,\mathrm{grad}\, C_\mathrm{D} \mathrm{d}\Omega + \int_\Omega \frac{\tilde{k}_{ij} u_j \underline{\omega}}{\|u\|} \underline{u} \,\mathrm{grad}\, C_\mathrm{D} \mathrm{d}\Omega = 0 \\
&\int_\Omega \frac{\tilde{C}_\mathrm{A} - C_\mathrm{A}^\mathrm{n}}{\Delta t} \mathrm{d}\Omega + \int_\Omega \omega \underline{u} \,\mathrm{grad}\, C_\mathrm{A} \mathrm{d}\Omega + \int_\Omega \frac{\tilde{k}_{ij} u_j \underline{\omega}}{\|u\|} \underline{u} \,\mathrm{grad}\, C_\mathrm{A} \mathrm{d}\Omega = 0
\end{aligned} \tag{4.26}$$

Nonlinearity

The discretization methods mentioned above are implicit and this leads to difficulties when solving a system of equations which has a large number of unknowns. The TELEMAC-System provides different types of solvers; only those used in this research are mentioned here. They are the Conjugate Gradient method, the Conjugate Gradient on Normal Equation method and the Generalized Minimal Residual method (GMRES). In addition to these solvers, the CTM-SUBIEF-2D module deals with five transport equations which are coupled through the interaction terms (underlined in Eqs. 4.20–4.22). This coupling is weak in transport equations (Hinkelmann 2002) and therefore, a linear solver using the Picard method is implemented. The number of sub-iterations for this method is limited to 100; however, in some cases less than 10 iterations are needed.

Boundary Conditions

The TELEMAC-System treats three types of boundary conditions which are Dirichlet, Neumann and no boundary condition (degree of freedom). The first boundary condition prescribes the concentration of substances at the inflow or outflow boundaries. The second boundary condition deals with defined diffusive fluxes over the boundaries. Normally these fluxes are prescribed using the concentration gradient. In most cases, the diffusive fluxes over the boundaries are set to zero. The third type of boundary condition is the easiest to deal with since there is no change in the corresponding transport equation.

Module Limitations

The module deals so far with short term simulations with relatively small time steps on the order of magnitude of seconds. In addition to this, the following items are not considered:

1. Physical processes such as flocculation and consolidation.
2. Complete sediment mixing layers (multi-layer model). However, the simplified concept used has given reasonable results as compared to field measurements (Westrich, this vol.).
3. Interaction between different contaminants and different sediment fractions.
4. Chemical and biological reactions.

To show the calibration, validation or even comparison with other numerical models is beyond the scope of this section. However, a real case application for a headwater section of the Upper Rhine where data on sediment properties (erosion), sediment depth profile, contaminated fraction and suspended sediment concentration were available is shown (Westrich, this vol.). The numerical results show a good agreement with field data.

Readers who wish to know the applicability of the module in more detail, for various real cases, are referred in the first instance to Jacoub 2004, Jacoub and Westrich 2004, 2006 which show comparisons of the module results with physical model results for a flood retention reservoir and with field measurements for the river Elbe.

4.1.4 Conclusions

This research presents the development of a two dimensional numerical module for contaminant transport in rivers. The new module, named CTM-SUBIEF-2D, has been developed on the basis of the TELEMAC-System. It describes the transport of dissolved and particulate contaminants in the water column and river bed with emphasis on first order sorption kinetics. By solving five partial differential equations, the depth averaged of suspended sediment and dissolved and particulate contaminants in the water column and the river bed are calculated. Sedimentation, erosion, mixing of sediments and degradation of contaminants processes are taken into account. The module handles the interac-

tion between one contaminant substance with one sediment fraction. The module handles the time-dependent variables and parameters such as particle settling velocity, concentration or flux of sediments, and depth dependent variables in sediments.

Numerical schemes such as Operator Splitting method and Stream Upwind/Petrov-Galerkin method (SUPG) for treating the transport equations are implemented. The five transport equations are coupled through interaction terms. Because of the weak coupling of the five transport equations, the Picard method for linearization is used. Westrich, this volume, shows an application of the developed module for a headwater section of the Upper Rhine and its numerical results with comparison to field measurements.

References

Beulleudy Ph, SOGREAH (2000) Numerical simulation of sediment mixture deposition Part 1: analysis of a flume experiment. Journal of Hydraulic Research 38(6)

Beulleudy Ph, SOGREAH (2001) Numerical simulation of sediment mixture deposition Part 2: analysis of a flume experiment. Journal of Hydraulic Research 39(1)

Brooks AN, Hughes TJR (1982) Streamline Upwind Petrov Galerkin formulations for convection dominated flows with particular emphasis on the Naiver-Stokes equations. Journal of Computer Methods in Applied Mechanics and Engineering 32:199–259

Carroll J, Harms IH (1999) Uncertainty analysis of partition coefficients in a radionuclide transport model. Journal of Water Research 33:2617–2626

Chapra SC (1997) Surface water-quality modelling. Mc Graw-Hill, New York

Di Silvio G (1991) Sediment exchange between stream and bottom: a four-layer model. Proceeding of the international Grain Sorting Seminar, Mitteilung der Versuchanstalt für Wasserbau, Hydrologie und Glaziologie, ETH, vol. 117, pp 191–196

EDF (2002) TELEMAC Modelling System, 2D-Hydrodynamics software, Principles manual-validation documents. Direction des Etudes et Recherches, Distributed by SOGREAH consultants, edn 5.0

Haag I (2003) Der Sauerstoffhaushalt staugeregelter Flüsse am Beispiel des Neckars – Analysen, Experimente, Simulationen. Mitteilung, Institute of Hydraulic Engineering (IWS), University of Stuttgart, No. 122

Hinkelmann R (2002) Efficient Numerical Methods and Information-Processing Techniques in Environment Water. Mitteilung, Institute of Hydraulic Engineering (IWS), University of Stuttgart, No. 117

Jacoub G (2004) Development of a 2-D numerical module for particulate contaminant transport in flood retention reservoirs and impounded rivers. Doctoral thesis, Institute of Hydraulic Engineering (IWS), University of Stuttgart, No. 133

Jacoub G, Westrich B (2004) 2-D numerical code to simulate the transport and deposition of dissolved and particulate contaminants in a flood retention reservoir. International Conference on Hydro-Science and Engineering, ICHE 2004, vol. 6, pp 272–274

Jacoub G, Westrich B (2006) Effect of river groyne structures on flow, sedimentation and erosion dynamics in rivers (Case study: the river Elbe). The International General Assembly Conference EGU-2006, Vienna-Austria

James A (1993) An Introduction to Water Quality Modeling. Second edition

Kelly DW, Nakazawa S, Zienkiewict OC, Heinrich JC (1980) A note of upwinding and anisotropic balancing dissipation in finite element approximations to convective diffusion problem. International Journal of Numerical Methods Engineering 15:1705–1711

Santschi PH, Honeyman BD (1989) Radionuclides in aquatic environments. Journal of Radiation Physics and Chemistry 34(2):213–240

Sieben A (1996) One dimensional models for mountain-river morphology. Communications on Hydraulic and Geotechnical Engineering, Delft University of Technology, Report no. 96-2

Thomann RV, Mueller JA (1987) Principles of Surface Water Quality Modelling and Control. Harper International edition

Joachim Karnahl · Bernhard Westrich

4.2 Two-Dimensional Numerical Modeling of Fine Sediment Transport Behavior in Regulated Rivers

4.2.1 Introduction

In most cases low flow velocities in the headwater of weirs and dams cause sedimentation of fine suspended sediments resulting in a reduction of the flow cross-section. In waterways, where the navigability is restricted and the safety of the embankments is affected, the deposited sediments must be removed. Since many river sediments are polluted by various substances, the dredging and disposal of contaminated sediments requires a feasibility study focusing on the environmental impact. A numerical transport model can provide basic information about the temporal and spatial distribution of the disposed sediments in the river channel, and their potential deposition in near bank river training structures such as groyne fields, or in harbours and cut-off meander.

A two dimensional depth averaged flow and transport model was developed to describe the transport, dispersion, sedimentation and erosion of different suspended sediment fractions as well as adsorbed and dissolved pollutants.

Contaminant transport modeling needs detailed information about suspended sediment concentration, fractional sediment fall velocity and sorption parameters. Field measurements of suspended sediment concentration, flow velocity and water level usually provide only local or cross-section averaged data which must be analyzed and evaluated for model calibration. In the field, remobilization and release of adsorbed substances to the aqueous phase is often not detectable because of chemical analysis limitations.

4.2.2 Objective

The objective of this study was to build a mathematical model to describe the processes of multifractional suspended sediment transport with adsorbed and dissolved contaminants for applications in surface waters. A depth averaged 2-D model was chosen in order to model longer time periods and larger domains. This model was applied to investigate the temporal and spatial distribution of three suspended sediment fractions, as well as the adsorbed and dissolved toxic substance *Hexachlorobenzoene* (HCB) in the plume of dredged material disposed in the tailwater of a hydro-power station at the Upper Rhine River. The model generates the concentration field and the sedimentation patterns and was used to perform a sediment mass balance. The uncertainties of the field data and the model results are discussed.

4.2.3 The Numerical Model

The hydrodynamic part of the simulation was performed by using the 2-D Finite-Element model TELEMAC 2D which solves the depth-averaged Saint-Venant equations and generates the flow field for the transport and reaction model SUBIEF 2D (EDF 2004).

Both models are independent from another, i.e. they are solved sequentially and not simultaneously. Different approaches for the bed roughness are implemented, similarly different turbulence models (constant viscosity, k-ε, Elder model), numerical schemes and solvers are available. The following section describes the basic mathematical equations for the transport model. The model domain and the model parameters are described in Sect. 4.2.4 and in Table 4.2.

Model Development

To simulate the transport of contaminated particles the SUBIEF 2D code was extended to model multifractional sorption processes, including the sedimentation and erosion processes of the particles with adsorbed substances. The model allows the implementation of chemical and biological reactions like transformation and degradation, as well as diffusive flux of the dissolved substances at the water-sediment interface. The basic model concept is shown in Fig. 4.4.

The 2-D transport equations for suspended sediments, dissolved and adsorbed substances are generally given in the following form:

$$\frac{\partial C_i}{\partial t} + \underline{u}\,\mathrm{grad}\,C_i = \frac{1}{h} div\left(h\underline{\underline{D}}\,\mathrm{grad}\,C_i\right) \pm \text{source/sink} \tag{4.27}$$

with C_i = concentration (kg m^{-3}) (suspended sediment, dissolved or adsorbed substances), t = time (s), u = velocity (m s^{-1}), $\underline{\underline{D}}$ = dispersion tensor (m^2 s^{-1}).

In the following case study the formulation of Elder (1959) is used for the dispersion coefficient:

$$D_{l,t} = u_* h k_{l,t} \quad \left(\frac{\mathrm{m}^2}{\mathrm{s}}\right) \tag{4.28}$$

with u_* = friction velocity (m s^{-1}), h = water depth (m), $k_{l,t}$ = calibration constants in longitudinal and transversal flow directions.

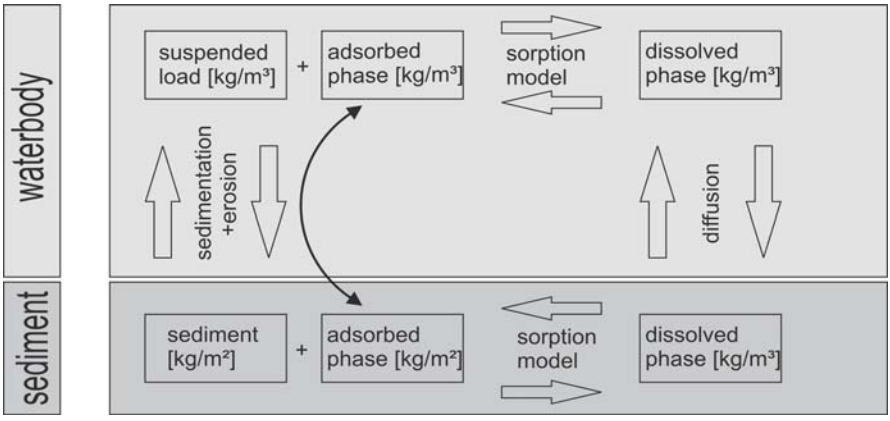

Fig. 4.4. Basic model concept

Erosion and deposition are the main source and sink terms in the suspended sediment transport equation. For the deposition of cohesive sediment the following formulation (Krone 1962) is used:

$$S_{i,\text{sediment}} = \begin{cases} w_{s,i}\, C_i \left(1 - \dfrac{\tau_0}{\tau_{\text{crit,Si}}}\right) & \left(\dfrac{\text{kg}}{\text{m}^2\text{s}}\right) \quad \text{for} \quad \tau_0 < \tau_{\text{crit,Si}} \\ 0 \qquad\qquad\qquad\qquad\qquad\quad \text{for} \quad \tau_0 \geq \tau_{\text{crit,Si}} \end{cases} \tag{4.29}$$

with $S_{i,\text{sediment}}$ = sedimentation rate of fraction i (kg m^{-2} s^{-1}), $w_{s,i}$ = respective fall velocity of fraction i (m s^{-1}), τ_0 = bed shear stress (N m^{-2}), $\tau_{\text{crit,Si}}$ = critical deposition shear stress of fraction i (N m^{-2}).

The sedimentation rate of the adsorbed substances $S_{i,\text{adsorbed}}$ associated with the fraction i depends on the ratio between the concentration of the adsorbed substance $C_{i,\text{adsorbed}}$ and the concentration of the suspended sediment $C_{i,\text{sediment}}$:

$$S_{i,\text{adsorbed}} = S_{i,\text{sediment}} \frac{C_{i,\text{adsorbed}}}{C_{i,\text{sediment}}} \quad \left(\frac{\text{kg}}{\text{m}^2\text{s}}\right) \tag{4.30}$$

The critical deposition shear stress can be approximately assumed constant or optionally described by the energy approach after Westrich and Juraschek (1985) by adaptation to multiple fractions as described by Dreher (2005):

$$\tau_{\text{crit,Si}} = \frac{(\rho_s - \rho_w) g h \sum w_{s,i}\, C_{i,\text{sediment}}}{k u \rho_s} \quad \left(\frac{\text{N}}{\text{m}^2}\right) \tag{4.31}$$

with g = gravity constant (m s^{-2}), k = bed form and grain size specific constant defined as required energy for suspension over available dissipative energy from the flow (–), ρ_s = sediment density (kg m^{-3}).

For the erosion of (cohesive) sediments the approach by Kuijper et al. (1989) based on Partheniades (1965) is used with adaptation to multiple fractions as follows:

$$E_{\text{total}} = \begin{cases} m\left(\dfrac{\tau_0 - \tau_{\text{crit,E}}}{\tau_{\text{crit,E}}}\right) & \left(\dfrac{\text{kg}}{\text{m}^2\text{s}}\right) \quad \text{for} \quad \tau_0 > \tau_{\text{crit,E}} \\ 0 \qquad\qquad\qquad\qquad\quad \text{for} \quad \tau_0 \leq \tau_{\text{crit,E}} \end{cases} \tag{4.32}$$

with E_{total} = erosion rate of all deposited sediment fractions (kg m^{-2} s^{-1}), m = erosion constant (kg m^{-2} s^{-1}), $\tau_{\text{crit,E}}$ = critical erosion shear stress (N m^{-2}). The fractional erosion rate depends on the percentage mass of the sediment fraction i in the active bed layer:

$$E_{i,\text{sediment}} = E_{\text{total}} \frac{M_i}{\sum M_i} \quad \left(\frac{\text{kg}}{\text{m}^2\text{s}}\right) \tag{4.33}$$

with $E_{i,\text{sediment}}$ = erosion rate of sediment fraction i (kg m^{-2} s^{-1}), M_i = mass of fraction i in the bed (kg).

The erosion rate of the adsorbed substances $E_{i,\text{adsorbed}}$ associated with the fraction i depends on the ratio between the mass of the adsorbed substance in the sediment $M_{i,\text{adsorbed}}$ and the mass of the sediment $M_{i,\text{sediment}}$:

$$E_{i,\text{adsorbed}} = E_{i,\text{sediment}} \frac{C_{i,\text{adsorbed}}}{C_{i,\text{sediment}}} \quad \left(\frac{\text{kg}}{\text{m}^2\text{s}}\right) \tag{4.34}$$

Chemical, biological and degradation processes are treated as user defined exchange terms for each substance. The Freundlich or Langmiur isotherms (Stumm and Morgan 1996) are usually used for sorption processes. In the following case study, the partitioning coefficient K_d, based on the Freundlich isotherm, with first order kinetics is implemented as follows:

$$J_{\text{sorption},i} = k_\text{t} \left(K_\text{d}\, C_{\text{S},i}\, C_\text{d} - C_{\text{A},i}\right) \quad \left(\frac{\text{kg}}{\text{m}^3\text{s}}\right) \tag{4.35}$$

with $J_{\text{sorption},i}$ = mass flux due to sorption (kg m^{-3} s^{-1}), k_t = kinetic sorption factor (s^{-1}), K_d = partitioning coefficient (l kg^{-1}), $C_{\text{S},i}$ = sediment concentration of fraction i (kg m^{-3}), C_d = dissolved concentration of a substance (kg m^{-3}), $C_{\text{A},i}$ = concentration of a substance adsorbed onto fraction i (kg m^{-3}).

4.2.4 Case Study: Disposal of Dredged Material

Site Description

In the headwater of the Iffezheim weir which is the lowest downstream hydropower station in the Upper Rhine River, fine cohesive sediments had to be removed to reestablish the original flow cross-section and to ensure the freeboard required for the safety of the embankment against flooding. The material was dredged by a suction dredger and disposed through a 3.5 km long pipeline to the tailwater during low water levels with a corresponding river discharge ranging from 700 to 1 500 m^3 s^{-1} to avoid sediment deposition on the flood plains. Measurements were performed before, during and after the dredging in the main channel, in typical groyne fields and harbor areas over a distance of 100 km. These included local flow velocities, suspended sediment concentration, grain size distribution and turbidity. Sediment traps were also deployed at different locations.

The numerical investigation is focused on the upper 22 km long river reach immediately downstream of the Iffezheim weir between river km (rkm) 334.0–356.2. The confluence of the Murg tributary is located 8 km downstream of the weir. Three gauging stations are inside the model area (Fig. 4.5): Iffezheim (rkm 336.6), Plittersdorf (rkm 340.3) and Lauterbourg (rkm 349.3). The measured discharge at Plittersdorf is used as the inflow boundary condition. Figure 4.5 shows a typical grain size distribution of the suspended sediment and the model area with the locations of the cross-sections at which measurements and gauging took place.

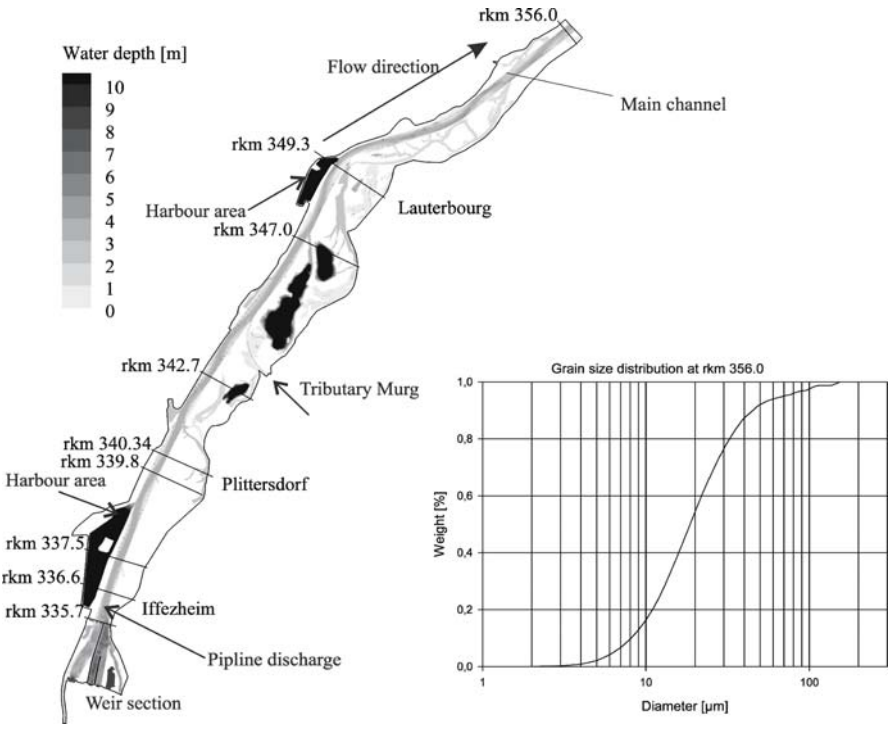

Fig. 4.5. General layout of tailwater section

Model Input Data from Field Measurements

During the dredging and disposal period, which lasted from Jan. 18 to Feb. 17, 2005, about 150 000 m^3 of sediment was discharged through the slurry pipeline. Figure 4.6 shows the discharge, the dredged material mass flux and the HCB concentration of the dredged material during the disposal period. During the dredging operation there was a flood in the Murg tributary from January 20–22, 2005 and a small flood in both the river Rhine and Murg from February 11–17, 2005. The variation of the mass discharge pumped by the dredger is caused by the temporary interruption of the suction dredger. Sediment samples were taken at the suction dredger to investigate grain size distribution, HCB concentrations and other chemical parameters of the dredged material. The percentage of sediment particles with a diameter greater than 200 µm was less than 5% by weight. Hence three sediment fractions 0–20, 20–60, 60–200 µm were modeled to consider different adsorbed HCB concentrations and different sedimentation behavior. Adsorbed HCB was found in all three sediment fractions. To overcome the heterogeneous grain size distribution and therefore also the adsorbed HCB concentration, cumulative samples were taken, indicated by the step like dashed line in Fig. 4.6, showing the HCB concentration. However the cumulative samples of the 3 fractions still show fluctuations in the fractional percentage, e.g., for the 20–60 µm fraction a range from 18.4 to 24.8% (see Table 4.1).

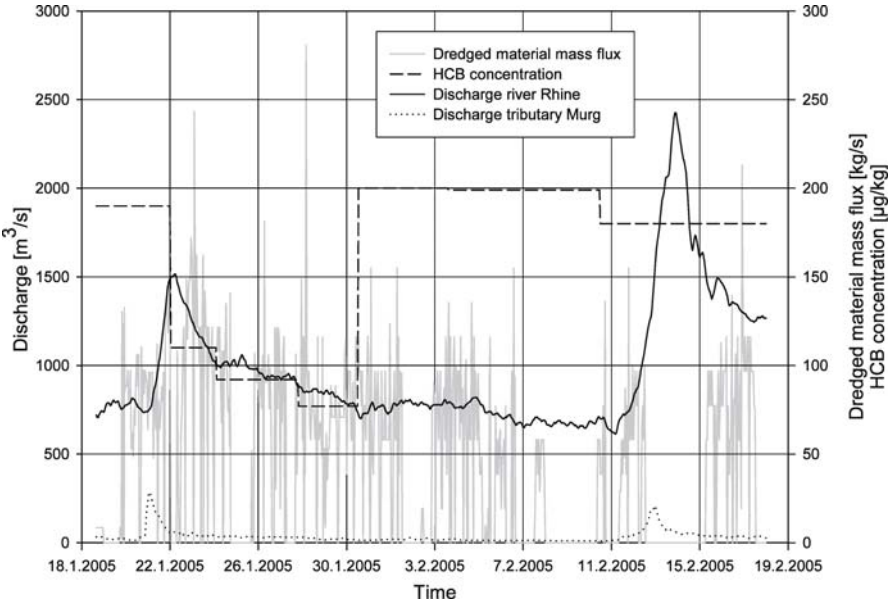

Fig. 4.6. Discharge, dredged material mass flux and HCB concentration of the dredged material

Table 4.1. Sediment distribution and HCB concentration

	Input data	0–20 µm fraction (%)	20–60 µm fraction (%)	60–200 µm fraction (%)	HCB concentration (µg kg^{-1})
Background	9 – 40 mg l^{-1}	42.0	46.5	11.5	85
Flushed sediment	0 – 280.6 kg s^{-1}	48.0 – 71.1	18.4 – 24.8	6.8 – 25.7	92 – 200

The background suspended sediment concentration in the Rhine was nearly constant at 9 mg l^{-1}, except for 7 days from February 11–18, 2005 with an increased background concentration up to 40 mg l^{-1} due to a high discharge of 2 425 $m^3 s^{-1}$. The adsorbed HCB background concentration has been monitored as 85 µg kg^{-1} and this value was used in the model calculations. Since no measurements in the Murg tributary exist, the background suspended sediment concentration is also assumed to be 9 mg l^{-1}. Since the dissolved HCB is below the chemical detection limit the background concentration was assumed to be zero.

Model Domain Description and Setup

The model domain area is ~29.3 km^2, and discretizised by 88 910 nodes with 175 870 elements. The smallest node distance is 1.6 m, the largest node distance is 63.6 m (mean ~15 m) the element areas range from 1.6 m^2 up to 1 274 m^2. The typical node distance in the main channel and the groyne fields is around 20 m, the groyne structures have a finer resolution with node distances from 1.6 to 10 m. The mesh resolution on the

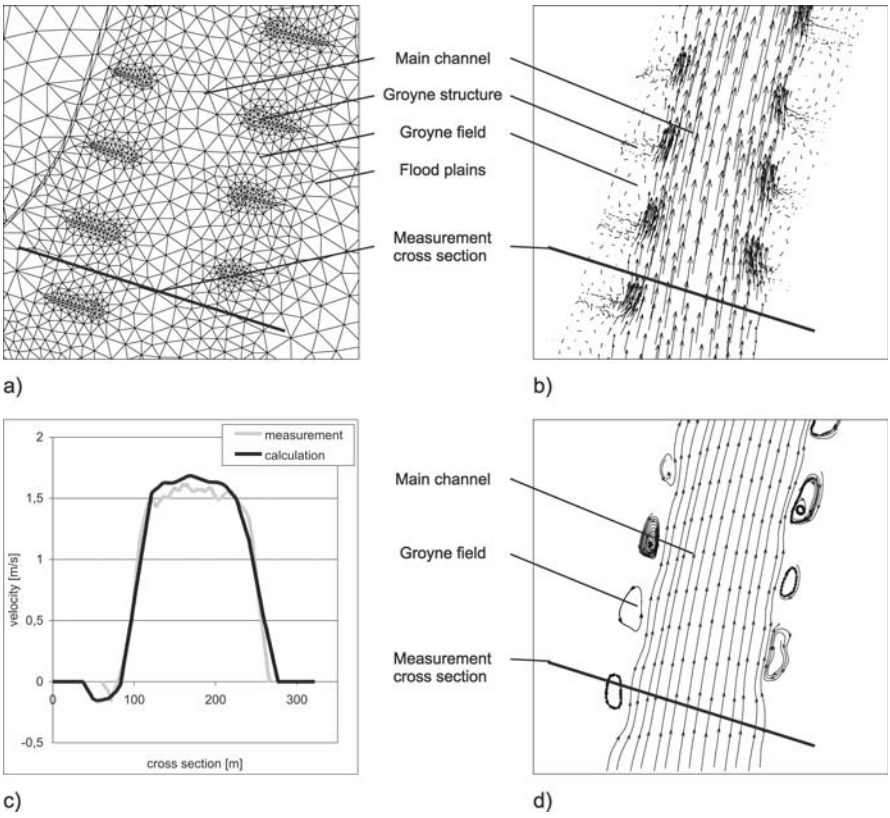

Fig. 4.7. a Mesh resolution, **b** flow field, **c** flow velocities, **d** streamlines

flood plains is larger than in the main channel, except the flow paths from small side streams. Figure 4.7a shows a mesh-section including the measurement cross-section at Iffezheim.

In a first step the hydrodynamic model for the flow field was calibrated with a steady state discharge and then applied to the 30 day unsteady flushing period with a time step of 5 seconds. The model run for the flow field took around 12 h computation time using 32 parallel processors.

In a second step the transport model should be calibrated but due to high fluctuation of the flushing mass and the available measured data a calibration cannot be performed, so different scenarios were calculated. A transport model run with 32 parallel processors took around 2.5 days computation time with a time step of 2 seconds.

The Flow Field

The tailwater at the weir is regularly fed with gravel to avoid bed erosion. Therefore, downstream of the weir there is some bed elevation change due to both the dumping of gravel material and bed load transport. The channel bathymetry was measured in the

fall of 2001. Several water level measurements were conducted. For the hydraulic model calibration the water level measurement of November 6, 2001 at a constant low flow discharge of 810 $m^3 s^{-1}$ was used, to minimize the effect of the sediment feeding on the bed elevation. The difference between calculated and measured water level is in the range of ±5 cm.

The unsteady flow model calculation for the 30 days flushing period (Discharge see Fig. 4.6) was compared with the data of the three gauging stations Iffezheim, Plitterdorf and Lauterbourg. At Iffezheim the calculated water levels differs between –49 cm to +30 cm compared with the measured values and have a root mean square error (RMSE) of 8.4 cm. At Plittersdorf the difference ranges from –31 to +29 cm (RMSE 6.8 cm) and at Lauterbourg from –21 to +32 cm (RMSE 6.0 cm).

The largest water level difference was observed during the rising phase of the small flood events. The discrepancy is mainly caused by the fact, that the data from Plittersdorf, which is 6 km downstream of the weir are used as upper model boundary condition although there is a time lag of about 1–2 h. By accounting for this time shift better model fit was achieved, e.g., at Iffezheim the water level differences will be reduced to –29 to +6 cm (less than 10% of water depth). Additionally it is evident that the sediment feeding during the 4 years period between the flow model calibration and application has changed the bed morphology and therefore has an impact on flow resistance and water level. A significant change of the river bed conditions can be detected immediately downstream of the sediment feeding area. However, this effect is decreasing with distance to the weir. Nevertheless, the comparison between the measured flow velocities (BfG 2005) and the calculated values shows a good agreement, the maximum difference is about 13%. Figure 4.7b show the flow field for a low flow situation of 780 $m^3 s^{-1}$, where the groynes are not overtopped, with high flow velocities in the main channel, eddies in the groyne fields and no flow on the flood plains. This can also be seen in Fig. 4.7d where the streamlines are shown. Figure 4.7c shows the measured and calculated velocities. The difference in the flow velocities in the groyne field results from the measurement method (ADCP), which enables only good measurements for higher flow depth. Finally, the model was calibrated for a steady state low flow situation (810 $m^3 s^{-1}$) and not for unsteady flow situations.

The Transport Model

The transport model describes the transport behavior of the three suspended sediment fractions in the main channel, in adjacent groyne fields and harbor areas. The model does not properly resolve the near-field mixing in the vicinity of the pipeline discharge because the resolution of the model in the vicinity would need to be considerably high. Similarly buoyancy effects and reducing mixing due to the highly concentrated suspensions discharged from the pipe were also not represented in the model. The simulation of the flow field has some uncertainties, which must be keep in mind for the interpretation of the transport model results. Flocculation processes where not taken into account, due to the fresh water conditions and the low concentrations in the far field of the dredged sediment.

Several simulations with different physical input parameters were done. An estimation of the sensitivity to the input parameters is thus possible.

Table 4.2. Physical parameters for the transport model variations

Parameter (Reference)	Unit	V 1	V 2	V 3	V 4	V 5	V 6
Fall velocity w_s (Zanke)	m s^{-1}	0.00009 (for 0– 20 µm) 0.00142 (for 20– 60 µm) 0.01390 (for 60–200 µm)					
Erosion constant m (Metha)	kg m^{-2} s^{-1}	0.00005					
Critical erosion shear stress $\tau_{crit,E}$	N m^{-2}	0.5	2	100	0.5	2	100
Critical deposition shear stress $\tau_{crit,S}$ (van Rijn, Westrich)	N m^{-2}	0.07	0.07	0.07	0.07	Eq. 4.31	Eq. 4.31
Calibration constant k_l (Elder)	–	6.0					
Calibration constant k_t (Elder)	–	0.6					
Partitioning coefficient k_d (Boguslavsky, WSA)	l kg^{-1}	0	0	0	13 000	0	0
Kinetic factor k_t (WSA)	1/s	0	0	0	1/86 400	0	0

The physical parameters were taken from literature values, all physical parameters used in each of the six simulations (V 1–V 6) are shown in Table 4.2. Simulation V 5 was done to evaluate the effect of sorption processes. The fractional distribution is described by the fall velocity and is calculated for the mean value of the diameter range (e.g., 10 µm for the 0–20 µm range).

In V 1 to V 3 the critical erosion shear stress is varied and was assumed to be the mean value between freshly deposited sediment and softly consolidated sediments in the river reservoirs (0.5 N m^{-2}) and normal consolidated sediments (2 N m^{-2}), or set to 100 N m^{-2} to simulate the maximum possible sedimentation rate. The critical deposition shear stress was assumed to be the mean value of the experimental data of van Rijn (1993), or taken from Eq. 4.32 in V 5 and V 6. The conservative assumption that no HCB sorption processes occur was chosen as a first approximation for the model variation V 1–V 3 and for V 5 + V 6. In the variation V 4 a mean value of k_d (13 000 l kg^{-1}) chosen from literature (Boguslavsky 2000 and WSA 2002) and a value of k_t (1/86 400 s^{-1}) chosen from literature (WSA 2002) were assumed. The dissolved HCB in the bottom has a minor influence on whole system, therefore diffusion at the sediment–water interface and sorption processes within deposited sediments were neglected.

Discussion of the Model Results

The transport rates in terms of kg s^{-1} at different cross-sections of V 1 were compared with the measured transport rates of the BfG (2005) and shown in Fig. 4.8. The concentration measurement were in the form of several turbidity measurements in a cross-

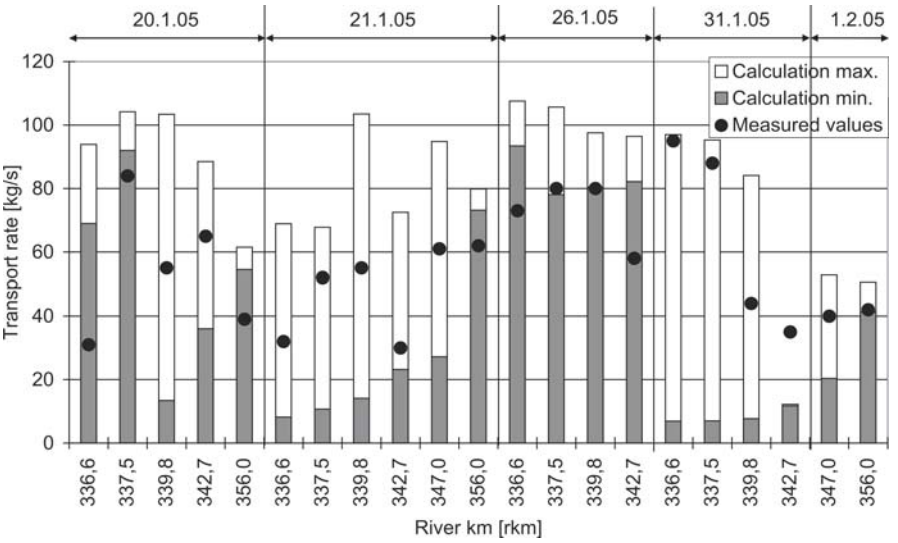

Fig. 4.8. Measured and calculated suspended sediment transport rates

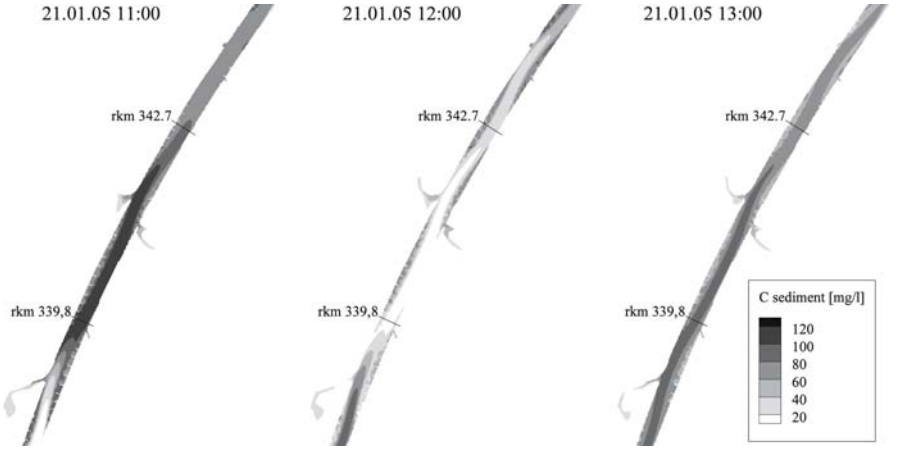

Fig. 4.9. Concentration fields

section. The turbidity sensor was calibrated at each cross-section with the suspended sediment concentrations determined from water samples. The transport rate is calculated by integration of the measured concentrations multiplied with the local flow velocity at the measurement point. During the survey the flow velocities and the concentrations substantially change in a given cross-section and therefore, the measurements do not represent an instantaneous concentration field and transport rate.

The calculated transport rates are instantaneous values and the minimum and maximum value in Fig. 4.8 represent the variation of the transport rate during the measurement period. The high variation of the calculated transport rates is caused by

the high fluctuation of the dredged material input and intermittent dredging activity, which makes a model calibration difficult. For instance Fig. 4.9 shows the concentration distribution from model results between the cross-section rkm 339.8 and 342.7 for three subsequent hours on January 21, 2005. At 11:00 a highly concentrated plume passing through rkm 339.8, resulting in a transport rate of 103.5 kg s^{-1} (Fig. 4.8), but one hour later the concentration there dropped dramatically so that the transport rate was only 14.1 kg s^{-1}. The measurements were taken between 11:00 and 12:00, therefore, a good agreement between the measured values and instantaneous model results cannot be expected and a model calibration cannot be performed.

Table 4.3 gives the total input mass (background values and disposed material together) and the percentage of deposited sediment mass and particularly deposited HCB mass.

Without taking sorption into account a good correlation of deposited sediments and deposited adsorbed HCB can be observed. The small difference results from the variation of the adsorbed HCB input concentration, the background value and the absence of particulate HCB input from the Murg tributary. As expected, a higher sedimentation of the larger particles was found. The variation of the critical erosion shear stress between V 1–V 3 (especially V 3 without any erosion) shows this effect more clearly. For fraction 3 an increase of sedimentation between V 1 and V 3 from 13.4 to 32.73% can be seen. Sedimentation mainly occurs near to the harbor entrance and in the groyne fields. Although the numerical mesh size in the side arms on the flood plains is very course, some deposition is still predicted.

By assuming sorption in V 4 a significant decrease of the deposited adsorbed HCB can be predicted. In the main channel a gradual increase of dissolved HCB (background value is zero) from the pipeline outlet to the end of the model domain due to desorption is calculated. But with the assumed sorption kinetic factor $k_t = 1/86\,400$ (s^{-1}) the residence time of 3–4 h in the main channel is not sufficient to reach the equilibrium state. Furthermore, a gradual dispersive release of dissolved HCB from groyne fields and harbor areas into the main channel during dredging breaks can be predicted. Analogously suspended sediments in the groyne fields are partly released in the main channel and partly deposited in the groyne field during dredging breaks.

Table 4.3. Total mass input and percentage of deposited sediment and HCB mass

	Fraction 1 (0–20 µm)	Fraction 2 (20–60 µm)	Fraction3 (60–200 µm)	HCB on Fraction 1	HCB on Fraction 2	HCB on Fraction 3
Total mass input	70 237 t	25 456 t	18 127 t	10.406 kg	3.821 kg	2.885 kg
Sed.V 1	2.11%	7.23%	13.40%	2.24%	7.12%	13.14%
Sed.V 2	2.26%	8.50%	18.19%	2.40%	8.51%	18.33%
Sed.V 3	2.86%	12.95%	32.73%	3.03%	13.33%	33.62%
Sed.V 4	2.08%	7.05%	13.09%	1.41%	5.90%	11.34%
Sed.V 5	3.32%	19.71%	43.28%	3.39%	19.07%	42.07%
Sed.V 6[a]	7.83%	38.97%	73.57%	8.24%	40.50%	74.58%

Comparing V 5 with V 2, which are only different by using an energy approach for the critical deposition shear stress (Eq. 4.31), shows a strong increase of sediment deposition in the groyne fields. This approach leads also to a strong deposition of suspended sediments in the main channel at the outlet of the flushing pipeline, which was observed in the nature but not found in V 1–V 4. The energy approach simulates the descent of the plume from the pipe onto the bed better than a constant critical shear stress. In V 5 and V 6 which use an energy approach, sedimentation is the dominating factor for all three fractions, whereas in V 1–V 3 the choice of the critical erosion shear stress has a stronger influence for the larger particles.

4.2.5 Conclusions

The 2-D transport model has proven to be a useful tool for a supplementary investigation and sensitivity analysis on the transport and sedimentation behavior of a contaminated suspended sediment plume in a navigational channel with groyne fields. The numerical study provides a deeper insight into the multifractional suspended sediment transport and physico-chemical processes as related to remobilization of adsorbed contaminants. Furthermore, it allows a calculation of the spatial and temporal contaminant distribution in the river system which could not be covered by the field data.

The present knowledge in modeling different sediment fractions is relatively poor, especially with respect to the erosion of separate fractions and need further research work. Nevertheless, the physical based numerical model is an engineering approach which enables a description of the most relevant physical processes, including sorption and degradation. However, more detailed and frequent field measurements are necessary to minimize the uncertainties of the physical and chemical parameters, especially the suspended particle settling velocity, the suspended sediment concentration and the pollutant specific sorption parameters. High spatially and temporally resolved data would also allow detailed calibration and validation of numerical models for predicting fine sediment transport in rivers.

Acknowledgments

We would like to thank the German Waterways and Shipping Office Freiburg (WSA) the German Federal Institute of Hydrology (BfG) and the German Federal Waterways Engineering and Research Institute (BAW) for their helpful cooperation. The investigation presented here was part of the project SEDYMO (*Se*diment *Dy*namic and *Mo*bility), funded by the German Federal Ministry of Education and Research (BMBF).

References

BfG (2005) Ergebnisse aus dem begleitenden Untersuchungsprogramm für die Umlagerung von Baggergut in die fließende Welle unterhalb der Staustufe Iffezheim/Rhein. BfG report 1474, Koblenz, in German

Boguslavsky S (2000) Orcanigc Sorption and Cation Exchange Capacity of Blacial Sand, Long Island. State University of New York, online published: http://pbisotopes.ess.sunysb.edu/reports/boguslavsky/

Dreher T(2005) Selektive Sedimentation von Feinstschwebstoffen in Wechselwirkung mit wandnahen turbulenten Strömungsbedingungen. Online published: http://elib.uni-stuttgart.de/opus/volltexte/2005/2263/; urn:nbn:de:bsz:93-opus-22633, in German
Elder JW (1959) The dispersion of marked fluid in turbulent shear flow. Journal of Fluid Mechanics 5(4):544–580
Electricite de France (EDF) (2004) TELEMAC modelling system. Distributed by SOGREAH consultants
Gualtieri C (2004) Interaction Between Hydrodynamics and Mass-Transfer at the Sediment-Water Interface. iEMSs: Manno, Switzerland, 2004. ISBN 88-900787-1-5
Krone RB (1962) Flume studies of the transport of sediment in estuarial shoaling processes. Hydr. Eng. Lab. and Sanit. Eng. Res. Lab., Univ. of California, Berkeley
Partheniades E (1965) Erosion and deposition of cohesive soils. Amer. Soc. Civ. Eng., J. Hydraulics Division, HY 1:105–139
Kuijper C, Cornelisse JM, Winterwerp JC (1989) Research on erosive properties of cohesive sediments. J. Geophysical Research 94(C10):14341–14350
Metha, AJ (1988) Laboratory Studies on Cohesive Sediment Deposition and Erosion. In: van Leussen W (ed) Physical Processes in Estuaries. Springer-Verlag Berlin Heidelberg New York, pp 427–445
Stumm W, Morgan JJ (1996) Aquatic Chemistry. Wiley-InterScience, New York Chichester Brisbane Toronto Singapore
van Rijn L (1993) Principles of sediment transport in rivers, estuaries and coastal seas. Aqua Publications Amsterdam Oldemarkt
Westrich B, Juraschek M (1985) Flow transport capacity for suspended sediment. International association for hydraulic research 21st Congress, Melbourne, vol. 3, pp 590–594
Westrich B (1988) Fluvialer Feststofftransport – Auswirkung auf die Morphologie und Bedeutung für die Gewässergüte. Oldenburg Verlag, München Wien, in German
WSA Freiburg (2002) Schlußbericht der Arbeitsgruppe "Baggerungen". Distributed by WSA Freiburg, in German
Zanke U (1982) Grundlagen der Sedimentbewegung. Springer-Verlag Berlin Heidelberg New York, in German

Dirk Ditschke · Mark Markofsky

4.3 A Non-Equilibrium, Multi-Class Flocculation Model

4.3.1 Introduction

Cohesive sediments build flocs which have settling velocities which are some orders of magnitude higher than those of the single particles. The floc size and thus the settling velocity depend on the turbulence intensity and the sediment concentration and properties. Generally it is assumed that a specific floc size is associated with a given flow regime or that at least the variance in the floc size distribution is small. In most cases only one sediment-class is used in models of suspended sediment transport in river or estuarine flow. In-situ and laboratory measurements show that this assumption may not be correct (Bornhold 1992). The floc size can vary an order of magnitude above or below the mean diameter. Therefore, it can be important to consider different sediment classes in order to refine and improve both deposition and suspended sediment concentration predictions. A special case where the consideration of different sediment classes is essential is the transport of polluted sediments since many pollutants are transported with the finest fractions.

The challenge of modeling multiple fractions of suspended sediment is that the flocs change their size due to flocculation and break-up. It is not sufficient to divide sedi-

ment into several fractions and compute the transport of each fraction. For flocculation and break-up processes it is necessary to consider an interaction between these fractions.

Although the flocculation time can play an important role in the prediction of sediment concentrations and deposition, the floc-size may be limited by the settling time (Winterwerp 1999). But also if the flow conditions change quickly, for example if sediment laden water flows from the rapidly flowing river into a harbor, the time which is needed to build up a floc-size equilibrium may be important for the deposition pattern in the harbor.

4.3.2 The Fractionated Flocculation Model

Interaction between Fractions

To meet this challenge the numerical model TELEMAC-3D (Hervouet 1991) was extended to treat different sediment classes. For each sediment class the three-dimensional transport equation is solved. Deposition and erosion are simulated for each class and the total bed evolution computed. Each sediment class is described by a settling velocity, w_s and a mean-particle diameter D. If only one parameter is available, the other is computed using Eq. 4.36 after Winterwerp (1998):

$$w_s = \frac{\alpha}{18\beta}\frac{(\rho_s - \rho_w)g}{\mu} D_p^{3-n_f} \frac{D^{n_f-1}}{1 + 0.15\mathrm{Re}^{0.687}} \tag{4.36}$$

The particles are assumed to be spherical ($\alpha = \beta = 1$), with a fractal dimension of $n_f = 2$. The primary particle diameter D_p is derived from measurements as the D_{50} of the non-flocculated sediment.

This equation is designed for cohesive sediments but works also for non-cohesive sediments by assuming spherical particles ($\alpha = \beta = 1$), with a fractal dimension $n_f = 3$ and a Stokes-regime ($Re \ll 1$). The settling velocity is the main parameter for the transport computation. The mean-diameter D of the sediment fraction is used for the exchange with the bed-morphology model SediMorph (Malcherek 2005).

With a multi-class sediment model it is possible to simulate a non-cohesive suspended load with a wide-spread size distribution or to follow specific sediment fractions. When combined with the bed-morphology model, the deposition of polluted sediment fractions can be simulated.

The second step is the simulation of cohesive sediment behavior through an interaction between the sediment classes. The flocculation process is simulated as an exchange from one sediment class into another with a higher settling velocity.

It is assumed that larger flocs always have a higher settling velocity and within each class all particles have the same diameter and settling velocity. In the other direction, break-up is defined as a transfer from one sediment class into another with a lower settling velocity and smaller diameter.

Of the different flocculation and break-up mechanisms in estuarine waters, turbulence induced flocculation and break-up is dominant (Winterwerp 1999). After a con-

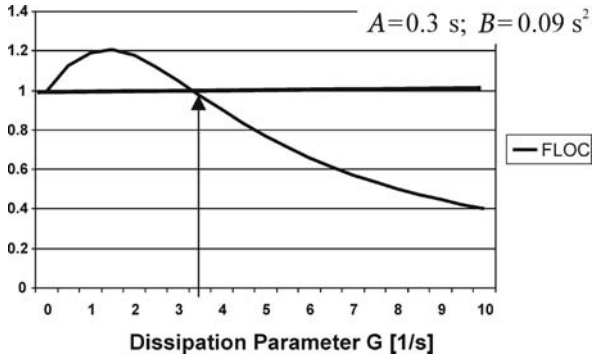

Fig. 4.10. Variation of the FLOC-parameter for increasing values of the dissipation parameter *G*

cept of Dyer (1989) flocculation increases with increasing turbulence due to the higher collision probability of flocs. With increasing turbulence, the shear stresses in the water rise and more and more flocs are destroyed. After a given turbulence intensity, break-up dominates flocculation. Based on the work of Argaman and Kaufman (1970), Van Leussen (1994) formulated this concept using Eq. 4.37 for the settling velocity w_s of cohesive sediments:

$$w_s = w_0 \frac{1 + AG}{1 + BG^2} \tag{4.37}$$

The dissipation parameter G (s^{-1}) = $(\varepsilon/\nu)^{1/2}$ is used to represent the turbulence intensity and can be computed with a k-ε-model. The parameters A and B are empirical values for flocculation and breakup; w_0 = settling velocity of a particular sediment class in still water.

The parameter FLOC (Eq. 4.38) is introduced to determine whether flocculation or break-up is dominant at a given turbulence intensity. At low G, FLOC becomes greater than 1 which leads to an increase in the settling velocity and indicates flocculation. At higher G FLOC becomes less than 1. The settling velocity decreases as break-up dominates.

$$\frac{1 + AG}{1 + BG^2} \equiv \text{FLOC} \rightarrow \text{FLOC} = \begin{cases} > 1 \rightarrow \text{Flocculation} \\ < 1 \rightarrow \text{Breakup} \end{cases} \tag{4.38}$$

Figure 4.10 shows the variation of the FLOC-parameter for increasing G. The values for the empirical parameter $A = 0.3$ s and $B = 0.09$ s^2 were determined through a calibration of the Weser Estuary (Malcherek et al. 1995) and do not necessarily apply to the general case.

Modeling of the Time Dependency

The flocculation process of cohesive sediment in nature at low concentrations is quite slow and can last several hours (Lick et al. 1992). The flocculation-time depends on the collision probability and the rate of collisions leading to growth of sediment flocs. Based

on the coagulation-theory (Smoluchofski 1917) the diameter of the floc has no major influence on the speed of the flocculation process. The collision probability is mainly dependent on the turbulence intensity and the sediment concentration, while the probability that particles stick together depends primarily on the sediment physical and biological properties. These properties are lumped in the concept of "stickiness" in which the Extracellular Polymer Substance (EPS) is supposed to have the greatest influence for mud flocs (De Brouwer et al. 2002; Fengler et al. 2004). Unfortunately, a coherent relationship between the EPS-concentration and the stickiness of the flocs does not yet exist.

Break-up of flocs is generally much faster than flocculation. The primary factors are the forces generated by turbulent shear and the resistance of the flocs against these forces. The resistance is also associated with "stickiness". Contrary to the flocculation process, the resistance against the external forces is dependent on the floc diameter.

The time-dependency is realized in the numerical model by transferring in each time step only a small portion of a sediment fraction into the next larger class. An effectiveness-factor for flocculation $\varepsilon_{\text{floc}}$ and one for break-up $\varepsilon_{\text{break}}$ are introduced. For a sediment fraction i which has a smaller fraction j and a larger fraction k, the change of the concentration due to flocculation is computed as follows:

$$\frac{\partial c_i}{\partial t} = \left(\varepsilon_{\text{floc},j}\, c_j - \varepsilon_{\text{floc},i}\, c_i\right) / \partial t \tag{4.39}$$

The formulation for break-up is similar:

$$\frac{\partial c_i}{\partial t} = \left(\varepsilon_{\text{break},k}\, c_k - \varepsilon_{\text{break},i}\, c_i\right) / \partial t \tag{4.40}$$

Within each time step the change of a concentration c_i in the case of flocculation is computed as the transfer of the smaller fraction j into the next larger fraction k. If break-up is dominant, (FLOC < 1) the change comes from the break-up of the larger fraction k into the smaller class j. As the sediment is only shifted from one class into another the conservation of mass is ensured.

The effectiveness-factor ε parameterizes the factors influencing flocculation or break-up. For flocculation $\varepsilon_{\text{floc}}$ includes the effects of the turbulence intensity, the concentration and stickiness. The turbulence computed as G and the concentration c have theoretically a linear influence on the flocculation velocity (Smoluchofski 1917). As Smoluchofski does not consider break-up this assumption has to be modified. Even if flocculation is dominant, break-up also takes place. The effect of break-up is considered in the FLOC-parameter, which is used to represent the influence of turbulence in the fractionated flocculation model. Flocculation and break-up are equal when FLOC = 1. The stickiness of the flocs is parameterized with K_1 and is used to calibrate the model. Thus the flocculation effectiveness, $\varepsilon_{\text{floc}}$ can be given by:

$$\varepsilon_{\text{floc}} = K_1(\text{FLOC} - 1)c \tag{4.41}$$

The break-up effectiveness, ε_{break} includes the turbulence intensity, stickiness, the floc diameter and a calibration parameter K_2:

$$\varepsilon_{break} = K_2\left(\frac{1}{FLOC} - 1\right)D \tag{4.42}$$

In nature the floc-size is limited by the Kolmogorov-length (Van Leussen 1997). The minimum size distribution is that of single particles. The Kolmogorov-length λ_0 can be computed with a k-ε-model from $\lambda_0 = (\nu^3/\varepsilon)^{1/4}$. If this length becomes smaller than the mean diameter of a sediment fraction, flocculation of smaller fractions is less than the break-up.

The determination of a lower limit for the floc size is more complicated. Due to the concept of settling velocity classes in the model there is no distinction between a single particle which cannot be broken by turbulent shear stresses and a small floc with the same settling velocity. It is not possible to define a minimum concentration for each fraction from an analysis of the single particle size distribution. For example, the concentration of the smallest fraction can decrease to zero because all small particles are bound in flocs and thus associated with a larger fraction. For this reason, the characteristic parameters of a size distribution D_{10}, D_{50} and D_{90} are used to ensure a proper minimum size distribution. The D_{10} defines the diameter which is larger than that of 10% of the particles, D_{50} and D_{90} are defined accordingly.

This is realized in the model as follows: if the actual D_{90} is smaller or equal to the minimum D_{90}, then break-up of flocs with a diameter larger than the minimum D_{90} is stopped. The same happens for flocs with a diameter between D_{50} and D_{90} at the D_{50}-border, and at the D_{10}-border for flocs between D_{10} and D_{50}.

Comparison with the Coagulation Theory

A first estimation of the quality of the flocculation model is found by comparing the numerical results with the theoretical values of the coagulation theory (Smoluchofski 1917). Therefore, a short overview of the theoretical solution of the coagulation theory is given here. Under the assumption that flocculation takes place between two flocculation classes, the variation of a floc class k over time can be written as:

$$\left[\frac{\partial c_k}{\partial t}\right]_{FLOC} = \frac{1}{2}\sum_{i+j=1}\beta_{ij}\bar{A}_{ij}c_i c_j - c_k\sum_{i=1}^{\infty}\beta_{ik}\bar{A}_{ik}c_i \tag{4.43}$$

The first term on the right hand side of Eq. 4.43 is floc growth due to the flocculation of flocs belonging to two smaller floc-classes i and j; the second term describes the reduction of class k due to flocculation into a larger fraction. The function β is the probability that the particles i and j collide and $\bar{A}$ the probability that a new floc is formed due to the collision.

It is possible to convert this general flocculation equation into Eq. 4.44 for the time-dependent concentration c_t of a floc-class with the concentration c_0 at $t = 0$ (Malcherek 1995):

$$c_t = \frac{c_0}{\left(1 + \left(\frac{\beta\bar{A}}{2}\right)\frac{6c_0}{\pi D^3\rho_s}t\right)} \tag{4.44}$$

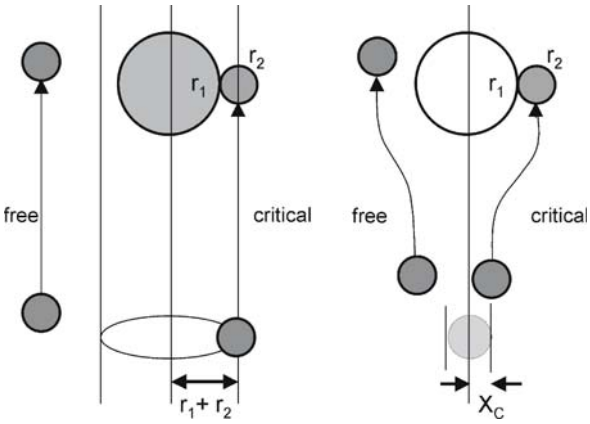

Fig. 4.11.
Schematic representation of the rectilinear (*left*) and curvilinear models (*right*) (after Han and Lawler 1992)

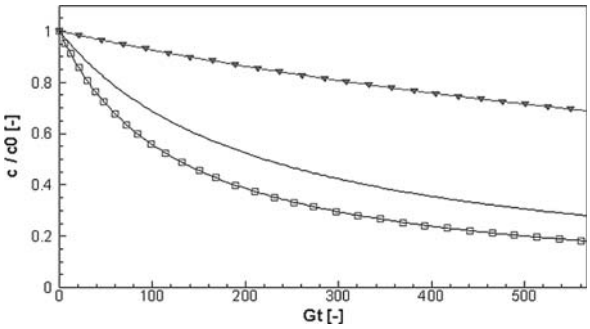

Fig. 4.12.
Comparison of the fractionated flocculation model (—) with the coagulation theory: rectilinear model (□); curvilinear model (◀)

For the collision probability β, different formulations have to be set depending on the collision mechanism. As we neglect the influence of Brownian motion and differential settling in estuaries, only the collision probability due to turbulence is considered:

$$\beta_{\text{Turb}} = \frac{G}{6}\left(D_i + D_j\right)^3 \tag{4.45}$$

It should be noticed that Eq. 4.45 overestimates the flocculation intensity and the settling velocity, because near-field effects are neglected. Laboratory experiments have shown that in the case of differential settling, the trajectories of small particles are deflected by larger particles. This leads to a major decrease of the collision probability (Stolzenbach and Elimelich 1994). Han and Lawler (1992) argued that this near-field effect is present even if two particles come close due to turbulent fluctuations. They proposed a "curvilinear model" with a correction-factor e_{cor} (Eq. 4.46) as an extension to the "rectilinear model" presented above:

$$e_{\text{cor}} = \exp\left[-3.4 + 0.62\log(\gamma) + \psi(3.5 - 1.2\log(\gamma))\right] \tag{4.46}$$

with $\psi = D_j/D_i$, $\gamma = 8H_A/(3\pi w_s D_i^2)$ and H_A is the Hamaker-constant, typically given as 3.9×10^{-20} for particles in water. Figure 4.11 demonstrates the different approaches for the rectilinear and the curvilinear models.

Additional investigations have shown that the rectilinear model overestimates the flocculation rate since near-field effects are neglected, but the curvilinear model underestimates the flocculation intensity because the permeability of the flocs is not taken into account (Li and Logan 1997). For this reason the results of the fractionated flocculation simulation introduced here should lie in between these two models.

Figure 4.12 shows a comparison between the fractionated flocculation model and both the rectilinear and the curvilinear coagulation theory models. For clarity, only the decrease in concentration of a floc class due to flocculation into a larger class is shown. The y-axis is normalized using the concentration at $t = 0$.

4.3.3 Analysis of Laboratory Experiments

The fractionated flocculation model was used to analyze laboratory experiments. The experiments were carried out at the Institute of Hydromechanics of the University of Karlsruhe (Kühn and Jirka 2006) within the "SEDYMO" research group (Fine *Se*diment *Dy*namics and Pollutants *Mo*bility in Rivers) (Förstner 2004). With a differential settling column (Fig. 4.13) it is possible to generate a controlled turbulence field similar to that of a natural river without having any advective transport.

The size distribution of kaolin flocs was measured with an inline microscope. By generating different turbulence profiles a regime with mainly flocculation was established as a flocculation test. Afterwards the turbulence was increased so that break-up was dominant in the whole water column. For a detailed description of the experiment see Kühn and Jirka (this volume). It should be mentioned, that the laboratory experiments where conducted at low concentrations, with low settling velocities when compared with natural flocs.

The set up of the numerical model differs from the laboratory test. Instead of a small tank without advection, a straight open channel with a constant velocity profile is used. The channel is 500 m long and 100 m wide to avoid boundary effects. Cyclic boundary conditions were prescribed in order to have the sediment concentration

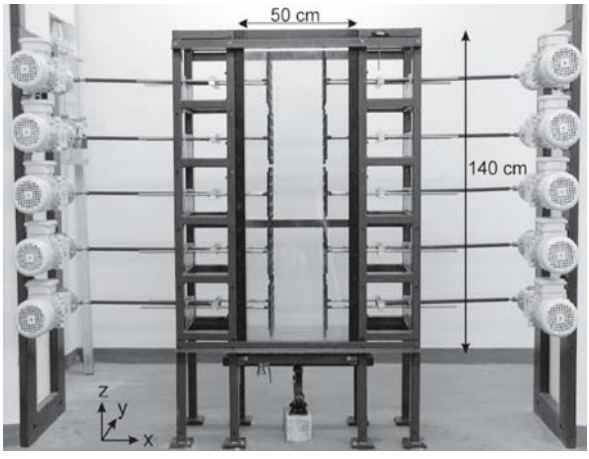

Fig. 4.13.
A differential settling column (Kühn and Jirka 2006)

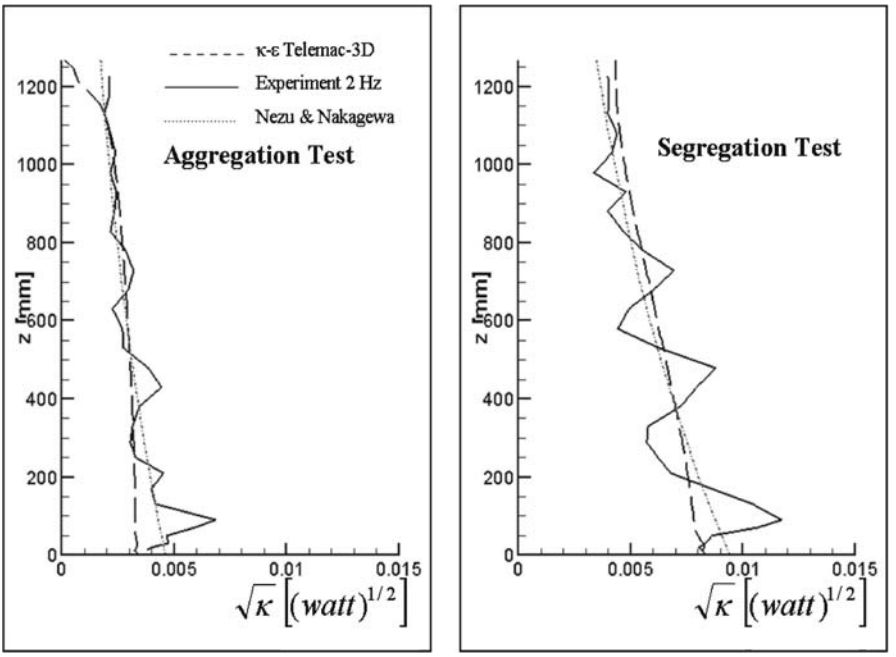

Fig. 4.14. Turbulence profiles of the numerical model, the experiment and theoretical values of Nezu and Nakagawa 1993 (*left:* aggregation; *right:* segregation)

independent of the advection. The same sediment mass flow which leaves the domain is added to the inflow as a boundary condition. The flow velocity is calibrated to meet the turbulence profile in the laboratory. Figure 4.14 shows the turbulence profiles calculated with the numerical model as well as the experimental data and the theoretical values of Nezu and Nakagawa (1993). In both the aggregation and the segregation test cases the flow velocities are quite low. In the numerical model, mean velocities of 5 cm s^{-1} for the flocculation case and 10 cm s^{-1} for the break-up case was chosen.

Aggregation

The laboratory experiments show that in the lower 40% of the water column break-up exceeds flocculation; at about 70% maximum flocculation is observed. With the numerical model the break-up is dominant for $G = 0.17\ s^{-1}$; the maximum flocculation at $G = 0.09\ s^{-1}$. The best fit of the flocculation parameters yielded $A = 3$ s and $B = 17\ s^2$. This shows that Kaolin-flocs are very unstable. For example, the boundary between flocculation and break-up in the Weser-Estuary was found to be at $G = 3.5\ s^{-1}$. Other laboratory flocculation experiments with artificial flocs use values for G of several hundred s^{-1} (Lick et al. 1992; Flesch et al. 1999).

An increase in the floc size was observed in the experiments after 4 hours. The floc-size distribution and the mean floc diameter were measured. In the numerical model,

Table 4.4.
Discretisation of floc fractions

D (µm)	%	C (mg l^{-1})	w_s (mm s^{-1})
5	2	0.010	1.80×10^{-2}
10	9	0.035	3.60×10^{-2}
15	32	0.115	5.39×10^{-2}
20	60	0.140	7.19×10^{-2}
30	90	0.150	1.08×10^{-1}
40	100	0.050	1.44×10^{-1}
60	100	0.010	2.16×10^{-1}

the floc-size distribution at the beginning of the experiment was discretized into 7 floc-size fractions (Table 4.4). The associated concentrations and settling velocities (Eq. 4.36) were computed with $\alpha = \beta = 1$, $n_f = 2$, $\gamma_s = 2.650$ kg m^{-3} and $D_p = 18.2$ µm.

The floc-size distribution after 4 hours in the model was compared with the experimental data at the location of maximum flocculation, i.e. at $z/h = 0.68$. The stickiness parameter for flocculation K_1 was adjusted to match the numerical results with the measured floc-size distribution (Fig. 4.15 and Table 4.5). Best results were achieved using a floc-size dependent stickiness. This seemed to indicate that smaller flocs have in this case a higher floc-building probability (see "Evaluation").

$$K_1 = \frac{0.7 \cdot 10^{-8}}{D^{1.6}} \tag{4.47}$$

Segregation

G is greater than 0.17 s^{-1} in the entire water column for the segregation test case, so break-up is dominant in the whole domain. In the experiment a steady state floc-size distribution was reached after 5 minutes. Since this distribution did not change after the turbulence intensity was increased, it can be concluded that all the flocs were destroyed. The numerical and measured floc-size distributions are in good agreement (Fig. 4.16 and Table 4.6). For break-up, the stickiness-parameter can be described by Eq. 4.48:

$$K_2 = 500 D^{1.25} \tag{4.48}$$

Evaluation

The numerical model can be used to analyze the results of the laboratory experiments. A relationship between the floc-size and the effectiveness of the flocculation and break-up processes was found.

The somewhat unexpected experimental result, that smaller flocs had a higher building capacity than larger ones is attributed to the nearly total lack of biological influences and the low concentrations and small particle and floc diameters in the

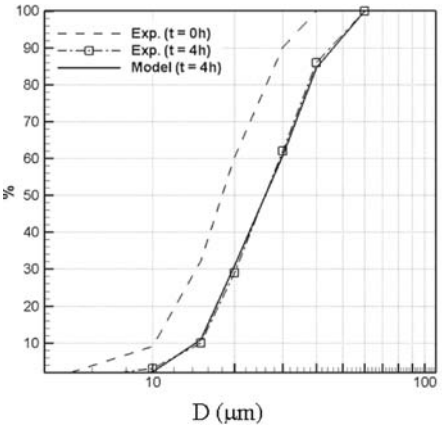

Fig. 4.15. The floc-size distribution after 4 hours in the flocculation experiment and in the numerical model

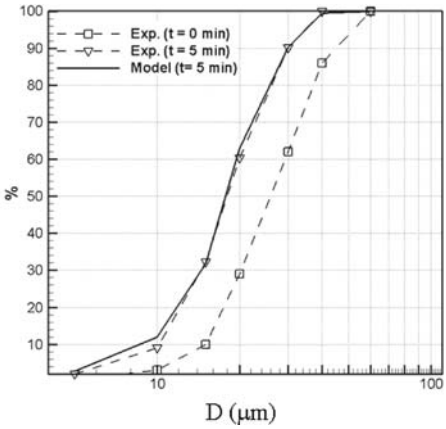

Fig. 4.16. The floc-size distribution after 5 minutes in the break-up experiment and in the numerical model

Table 4.5. Comparison of numerical and experimental results for flocculation

D (µm)	Size dist. (%) Exp. $t = 0$	Size dist. (%) Exp. $t = 4$ h	Size dist. (%) Model $t = 4$ h
5	2.0%	0.5%	0.1%
10	9.0%	3.0%	2.1%
15	32.2%	10.0%	10.9%
20	60.3%	29.0%	30.8%
30	90.1%	62.0%	60.8%
40	100.0%	86.0%	84.5%
60	100.0%	100.0%	100.0%
D_{50}	18.2 µm	26.4 µm	26.4 µm

Table 4.6. Comparison of numerical and experimental results for break-up

D (µm)	Size dist. (%) Exp. $t = 0$	Size dist. (%) Exp. $t = 5$ min	Size dist. (%) Model $t = 5$ min
5	0.1%	2.0%	2.7%
10	2.1%	9.0%	12.0%
15	10.9%	32.2%	31.8%
20	30.8%	60.3%	62.9%
30	60.8%	90.1%	90.3%
40	84.5%	100.0%	99.5%
60	100.0%	100.0%	100.0%
D_{50}	26.4 µm	18.2 µm	17.9 µm

experiments. The main influence for the stickiness is then not the biology but electrochemical forces, which are more effective for smaller particles.

Nevertheless, further investigations are necessary due to given uncertainties. Uncertainties can originate from the measuring technique since single flocs which appear in a small frame are counted and the probability of catching one of the bigger flocs is quite low. As such, the largest fractions may be underestimated. The choice of the discretization of the fractions in the flocculation model may influence the empirical parameters.

The flocculation model does not simulate a pure flocculation process. Using Eq. 4.38 for the FLOC-parameter always computes a kind of balance between flocculation and

break-up. Flocculation is therefore always dependent on break-up to a certain degree. It is possible that a floc-size dependency of the flocculation process can be deduced from the floc-size dependency of the break-up process.

4.3.4 Application to Sedimentation in an Estuarine Harbor

As an example for the simulation of sedimentation in an estuarine harbor, the Koehlfleet in the Hamburg Harbor area was selected. In 1990, a current deflection wall (CDW) was built at the harbor mouth to reduce sedimentation. The Hamburg Port Authority claims an average annual reduction of the harbor sedimentation of about 35% over a 6-year period.

In order to calculate the effect of such a wall in other harbor basins, a research project was started in 2001 to simulate this process with a numerical model (Ditschke and Markofsky 2003). The results showed a good representation of the flow fields with and without the CDW and of the water exchange between the estuary and the harbor; but the comparison between the computed and measured sedimentation showed a need for improvement. Therefore, the flocculation model described above was applied to the harbor model.

The data base in this area is quite good for flow and sediment. But floc size distributions were available for only one day (Bornhold 1992). From these measurements and the known average conditions for sediment concentrations and properties, initial values for the computation were extrapolated. The measured floc size distribution is simulated with 6 fractions. The largest fraction is set at the value of the Kolmogorov length computed with the turbulence model. The tabulated concentrations are average concentrations for flood and ebb tide (Table 4.7). The settling velocity for each fraction is computed from Eq. 4.36.

Initial numerical tests with a straight channel were conducted to roughly calibrate the parameters of the multi-class flocculation model. Reasonable results were found for:

$$\frac{1 + 0.5G}{1 + 0.07G^2} = \mathrm{FLOC} \tag{4.49}$$

Table 4.7.
The settling velocity for each fraction after Winterwerp (1999)

D (μm)	w_s (mm s^{-1})	Conc. Ebb (mg l^{-1})	Conc. Flood (mg l^{-1})
5	0.08	7	10.5
15	0.24	8.2	12.3
50	0.80	8.2	12.3
150	2.27	16.4	24.5
180	3.55	52.6	78.8
500	6.10	12.9	19.3
1 000	9.68	0.01	0.01

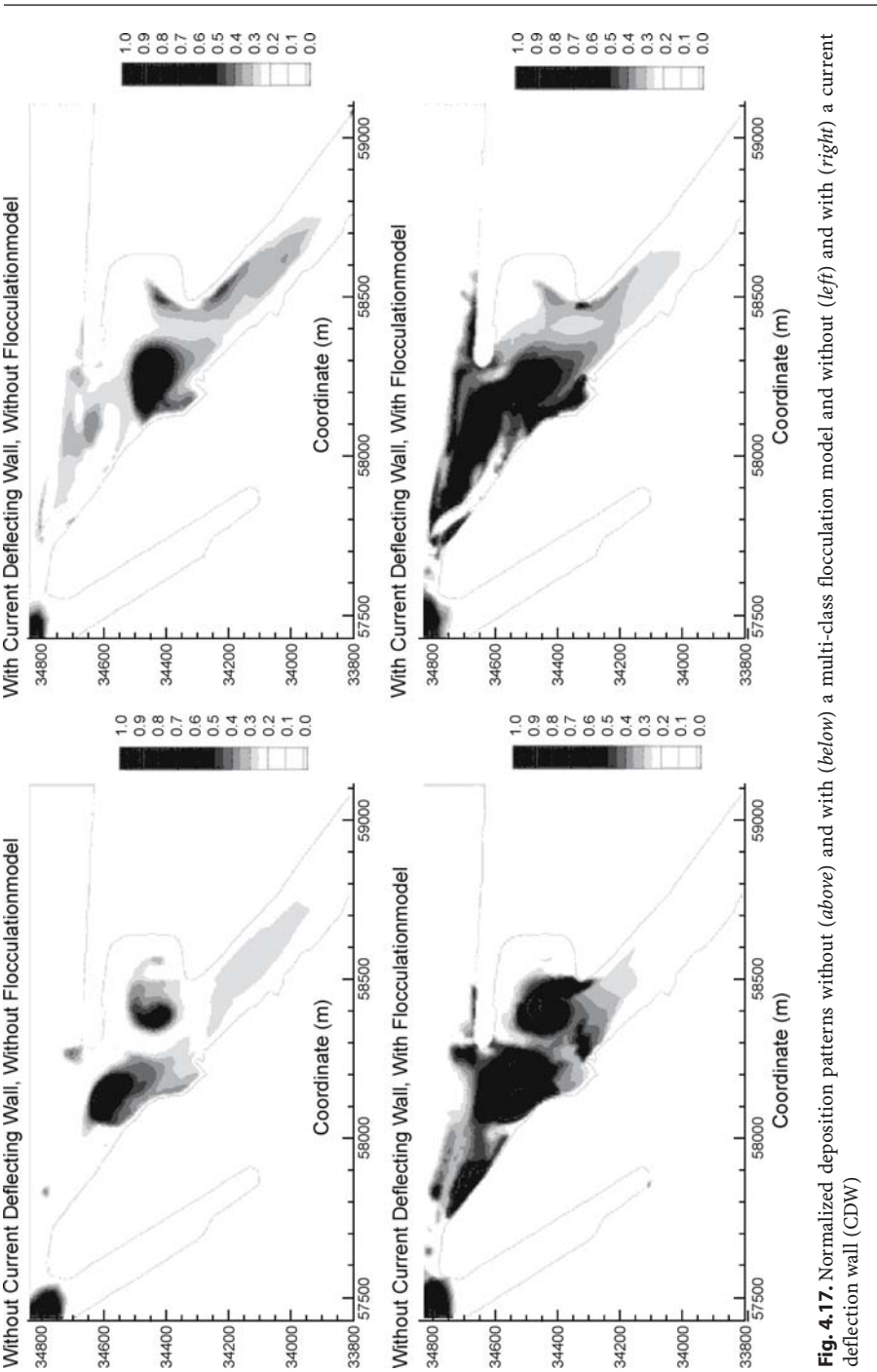

Fig. 4.17. Normalized deposition patterns without (*above*) and with (*below*) a multi-class flocculation model and without (*left*) and with (*right*) a current deflection wall (CDW)

Table 4.8.
Deposition (m^3) with and without a multi-class flocculation model and with and without a current deflection wall (CDW)

	1-Class flocculation	Multi-Class flocculation
Without CDW	1 690	2 710
With CDW	1 840	2 300
Difference	150	−410
%	+9%	−15%

The values for $A = 0.5$ and $B = 0.07$ are considered to be realistic because they are much closer to the values found by Malcherek et al. (1995) ($A = 0.3$ S; $B = 0.09$ S^2, see Fig. 4.10) than the values for the artificial sediment mentioned above.

The sedimentation during a single tide was computed with and without the multi-class flocculation model and with and without the current deflection wall. The results with this model show a reduction of 24% in the calculated deposition (Table 4.8) when compared with the 1-class simulation. The sedimentation patterns are also significantly different (Fig. 4.17).

The deposition is much higher in the computation with segmented flocculation model because the fraction with the largest settling velocity is not explicitly represented in a 1-class simulation but rather created by the flocculation model in areas with low turbulence (Kolmogorov length > 1 mm) i.e. within the harbor. Naturally a high settling velocity leads to increased sedimentation.

The calculated 15% reduction in sedimentation with the CDW during a single tide is of the same order of magnitude as the mean 6 year annual decrease of 35% stated by the authorities. Although one can not expect to hit the long term annual average with the computation of one single tide, this result indicates that the reproduction of the sedimentation processes in the harbor entrance is much better when one uses a segmented flocculation model.

To further understand the reasons for the improvement it is worth taking a closer look at the turbulence distribution near the harbor bottom and at the harbor entrance.

Figure 4.18 shows the dissipation parameter G at 5 cm above the bottom for both runs with and without a deflecting wall. At places where G is larger than (approximately) 7 Hz, break-up dominates flocculation. But even more important in this context is the Kolmogorov length (λ_0). If $G > 1$ Hz, λ_0 is <1 mm, and the largest flocs break. If $G > 4$ Hz, 0.5 mm flocs will also break. With a deflection wall, these values were exceeded over extensive bottom reaches and also in the middle of the water column. Values of about 3 Hz can be seen in the deflection channel and values for $G > 7$ in the vortex region of the wall.

4.3.5 Conclusions

At present three-dimensional numerical models generally use either one suspended sediment class with an advanced settling velocity formulation or use a multi-class

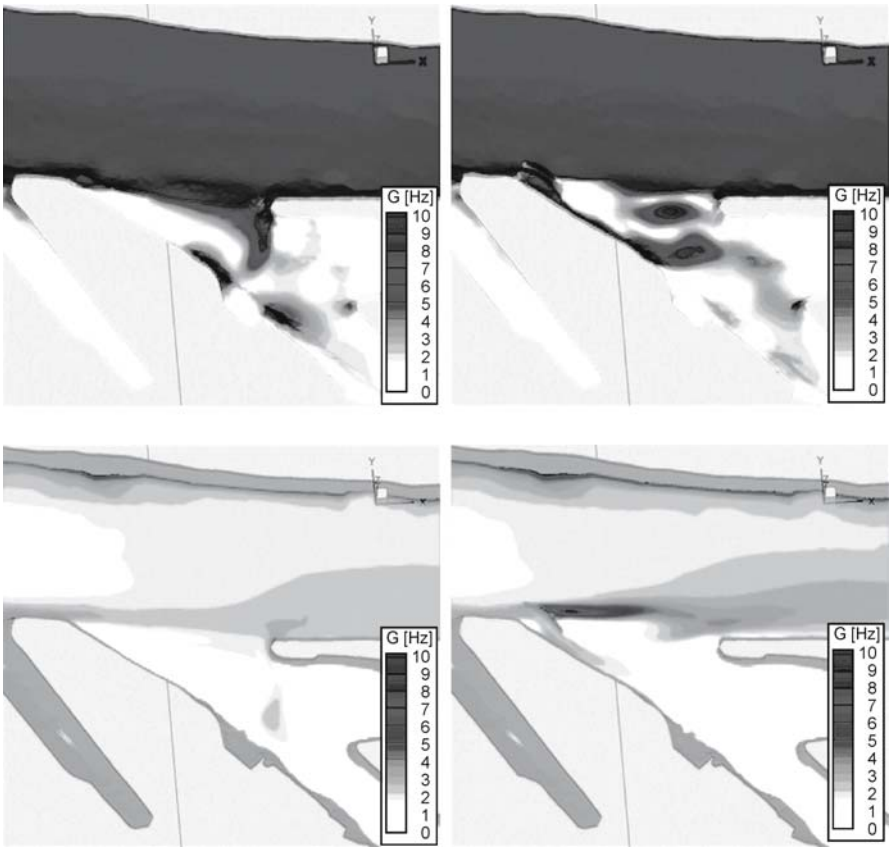

Fig. 4.18. The dissipation parameter G 5 cm above the bottom (*above*) and in 8 m water depth (*below*) without (*left*) and with (*right*) a CDW

approach for the different fractions of suspended sediment. The restriction in such models is that they either do not have the capability of dealing with a wide spread floc- or particle-size distribution or they cannot react to changing hydrodynamic conditions which generate a strong change in the floc-size distribution.

In order to refine and to improve suspended sediment concentration and deposition predictions, the numerical model Telemac-3D was extended to treat multiple classes of suspended sediment. The model presented here simulates the particle size distribution. For example, it is now possible to be consistent with a fractionated bed morphology model and to consider flocculation processes by calculating the generation of larger floc classes out of the primary particles. The time-dependence of the flocculation and breakup processes was implemented using an empirical effectiveness-parameter.

The calculations were found to be in good agreement with theoretical values and laboratory data and significantly improved predictions for harbor deposition.

Acknowledgments

The investigations presented here were part of the project SEDYMO (*Se*diment *Dy*namic and *Mo*bility) funded by the German Federal Ministry of Education and Research (BMBF).

References

Argaman Y, Kaufman WJ Turbulence and Floculationt. J Sanitary Engineering ASCE 96(SA2):223–241

Bornhold J, Puls W, Kühl H (1992) Die Flockenbildung von Elbeschwebstoff: Untersuchungen mit Fraktionen unterschiedlicher Sinkgeschwindigkeit. GKSS-Forschungszentrum

De Brouwer JFC, Ruddy GK, Jones TER, Stal LJ (2002) Sorption of EPS to Sediment Particles and the Effect on the Rheology of Sediment Slurries. Biogeochemistry(61), 57–71

Ditschke D, Markofsky M (2006 in Print) A Time Dependent Flocculation Model Intercoh 2005

Dyer KR (1989) Sediment Processes in Estuaries: Future Research Requirements. J Geophys Res 94(C10): 14327–14332

Fengler G, Köster M, Meyer-Reil LA (2004) Charakterisierung mikrobieller Lebensgemeinschaften in resuspendierten Sedimenten. SEDYMO-Workshop: Feinsedimentdynamik und Schadstoffmobilität in Fließgewässern, pp 25–26

Flesch JC, Spicer PT, Pratsinis SE (1999) Laminar and Turbulent Shear-Induced Flocculation of Fractal Aggregates. American Insitute of Chemical Engineers 45(5):1114–1124

Förstner U (2004) Sediment Dynamics and Pollutant Mobility in Rivers: An Interdisciplinary Approach. Lakes and Reservoirs: Research and Management (9):25–40

Han M, Lawler DF (1992) The (Relative) Insignificance of G in Flocculation. J Am Water Works Ass 84(10):79–91

Hervouet JM (1991) TELEMAC, a Fully Vectorized Finite Element Software for Shallow Water Equations. Second International Conference on Computer Methods and Water Resources

Kühn G, Jirka GH (2006) Fine Sediment Behavior in Open Channel Turbulence: an Experimental Study. Intercoh 2005

Li X, Logan BE (1997) Collision Frequencies of Fractal Aggregates with Small Particles in a Turbulently Sheared Fluid. Environmental Science Technology 31(4):1237–1242

Lick W, Lick J, Ziegler K (1992) Flocculation and its effect on the vertical transport of fine-grained sediments. Hydrobiologia (235/236):1–16

Malcherek A (2005) Mathematical Module SediMorph – Validation Document Version 1.1. In Technical Report. Bundesanstalt für Wasserbau

Malcherek A, Markofsky M, Zielke W (1995) Numerical Modelling of Settling Velocity Variations in Estuaries. In: Arch. Hydrobiol. Spec. Issues Advanc. Limnil 47:353–362

Malcherek A (1995) Mathematische Modellierung von Strömungen und Stofftransportprozessen in Ästuaren, Institut für Strömungsmechanik und elektronisches Rechnen im Bauwesen, Universität Hannover, Bericht Nr. 44/1995, Hannover

Nezu I, Nakagawa H (1993) Turbulence in Open Channel Flow. IAHR/AIRH Monograph Series Balkema Publishers, Rotterdam

Smoluchofski M (1917) Versuch einer Mathematischen Theorie der Koagulationskinetik Kolloider Lösungen. Zeitschrift für Physikalische Chemie 92:129–168

Stolzenbach KD, Elimelich M (1994) The Effect of Density on Collision Between Sinking Particles: Implication for Particle Aggregation in the Ocean. Journal of Deep Sea Research I 41(3):469–483

Van Leussen W (1994) Estuarine Macroflocs and their Role in Fine-Grained Sediment Transport. Dissertation, University of Utrecht

Van Leussen W (1997) The Kolmogorov Microscale as a Limiting Value for the Floc Size of Suspended Fine-Grained Sediments in Estuaries. Cohesive Sediments, pp 45–62

Winterwerp JC (1998) A Simple Model for Turbulence Induced Flocculation of Cohesive Sediments. Journal of Hydraulic Engineering Research 36(3):309–326

Winterwerp JC (1999) On the Dynamics of High-Concentrated Mud Suspensions. Dissertation, TU Delft

Michel Verbanck · Aurélie Larcy · Nicolas Huybrechts · Jean-Pierre Vanderborght

4.4 Suction-Vortex Resuspension Dynamics Applied to the Computation of Fine-Particle River Fluxes

4.4.1 Addressing the Fine-Particle Issue

River and estuarine management on the basin scale is receiving renewed attention in the agenda of EU member states, mainly under the prescriptions of the 2000/60 Water Framework Directive. One of the important components of the 'ecological status' to be reached in surface water obviously derives from the interaction processes between the dissolved and the particulate phases. In terms of pollutant transfer, particles with the finest sizes are those that cause the greatest environmental concern (Kausch and Michaelis 1996; Owens et al. 2005). To explore the various management options, environmentally oriented numerical river models should therefore be able to reproduce the transfer fluxes of these fine particles (Förstner 2004).

In this context, a first problem is that a part of this suspended particulate matter (SPM) can be transported as wash-load (WL) or very fine particle load, notably in a state of autosuspension. According to Bagnold (1962), autosuspended particles have a settling velocity w_s not exceeding the value US (i.e. the product of mean stream velocity U and slope of the energy grade line S). Among environmentalists, it is widely recognized that these fine (slow-falling) particles are key vectors of pollutants in river basins because of their specific surface and adsorption capacity. In the following it will be shown that there are serious shortcomings in the modeling options currently available (Rendon-Herrero 1974; Wang 1979) for accounting consistently for wash-load particle fluxes. Distinguishing, in a given SPM record, what can be designated as WL is one thing; being able to predict the WL flux as a function of the hydrological sollicitations developing in the course of years (or decades) in the river watershed is another, certainly more difficult, proposition.

A second difficulty in this area is that a small number of storm events of very high intensity, lasting only a few days, can deliver the largest fraction of the annual particle flux at a considered river cross-section (Salomons and Brils 2004). In these circumstances, the whole riverbed moves rheologically, a key feature not adequately accounted for in traditional hydraulic models (Yen 2000). In more general terms, there is no sufficient consideration of the dynamical equilibrium between alluvial channel resistance, bedform development and bed-material load discharge, and for the role turbulence plays in these feedback interactions (Cao and Carling 2002; Verbanck 2004a; Huybrechts and Verbanck 2006). To address the issue, a research action is underway in the framework of the EU Integrated project Aquaterra under FP6. Model development is based on vortex-drag concepts recently proposed by Verbanck (2006) as a viable option for predicting resistance-to-flow in alluvial streams displaying a dynamic bed morphology evolution. This opens new perspectives for simulating the transport of SPM in open-channels, acknowledging the role of suction vortices (Dinkelacker 1982) in actively maintaining the resuspension process. The concept is physically based and has, up to now, been applied with some success to a number of well documented fluvial systems. It has the advantage of significantly lowering the number of model parameters to be calibrated (see Sect. 4.4.3).

4.4.2 Approach

What Is Meant by 'Wash-Load' in This Study

Historically, the transport of bed material, either over the bed or in suspension, was categorized as 'bed-material load' while the very fine suspended sediments not present in appreciable quantities in the bed were designated as wash-load (Einstein 1950). When suspended load (SL) is distinguished from bed-load (BL), the classification is conceptual; it is the mode of transport which is used to make the distinction. Unfortunately, the definition of washload is considerably more ambiguous. On one side, the classification is based on the origin of the particles (coming from the watershed or from upstream river stretches, as opposed to the local riverbed). On the other side, 'not present in appreciable quantities' often means considering all grains of a size less than, for example, the d_{10} of the riverbed material to be wash-load (Einstein 1950). The problem is evidently that the two criteria do not necessarily match. An alternative perspective on very fine SPM transport is to identify the fall-velocity threshold under which particles are likely to be maintained in the water column by the autosuspension process (Bagnold 1962; Wang 1979). This is an interesting approach to the problem, as it more clearly introduces a dynamic threshold, less static (as a systematic use of the d_{10} criterion mentioned above). Along a similar line of thought, we choose in this study to have a purely empirical definition of wash-load (section below). The originality of the approach is that it starts from the dynamics of what is observed in suspension (irrespective of the grain size characteristics of the local riverbed). Adopting a dynamical threshold between wash-load and suspended load evidently implies that exchanges between the two components occur on a regular basis, both in the temporal and spatial frame. This is a well-known difficulty of the problem, especially in the estuarine environment, where a large part of the very fine suspensions are cohesive and have a tendency to form flocs, directly influencing their settling properties (ten Brink 1997; Chen et al. 2005; Desmit et al. 2005). All mentions of 'wash-load' in this contribution thus correspond to the working definition given as Eq. 4.50 (meaning i.e. that wash-load and suspended load are mutually exclusive).

Identifying 'Wash-Load' Contributions in Experimental Records

The coarse particles moving in permanent contact with the riverbed (q_{BL}), characterized by high settling velocities in the turbulent fluid medium ($w_s/u_* \geq 3$), are known to be predominantly inert (granular) and are therefore not taken into account explicitly here:

$$\text{observed SPM flux} = q_{\mathrm{WL}} + q_{\mathrm{SL}} \tag{4.50}$$

The total flux of suspended particle material observed in the water column at a given river location is thus perceived as the sum of two fluxes which, in a 1-D (low-concentration) perspective as adopted here, can be seen as the product of flow discharge Q ($\mathrm{m^3\,s^{-1}}$), volumetric concentration (either C_{WL} or C_{SL}) (–) and particle

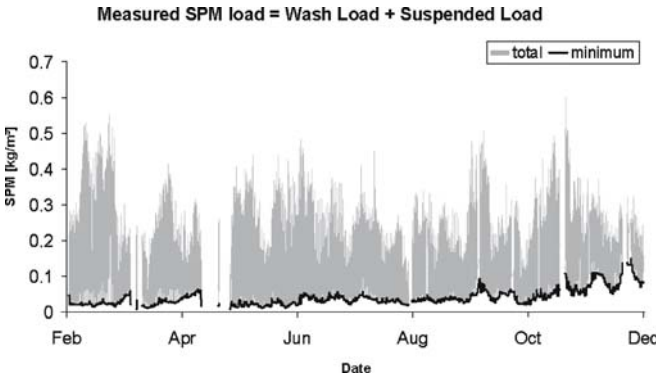

Fig. 4.19.
Eleven months of continuous turbidity records in the Scheldt Estuary

density ρ_s (kg m^{-3}). A typical distribution between $\rho_s C_{WL}$ and $\rho_s C_{SL}$ from an experimental survey of the tidal river Scheldt (Antwerp site, St. Anna landing stage) is illustrated on Fig. 4.19. Wash-load contributions will be the highest when high discharges from the upstream watershed (November and December in this case) have been able to mobilize pollutant sources distributed on the surfaces exposed to runoff. However, as highlighted by Symader et al. (this volume), the runoff remobilization process can present strong local features, with the most intense events not necessarily associated with the highest wash-load fluxes.

In this estuarine case, a technique has been found to overcome the difficulty of having q_{WL} and q_{SL} unresolved in the SPM records. As the stream velocity reverses twice per tide, the minimum observed SPM concentration during a tidal cycle corresponds to a slack with velocity dropping to zero. The minimum concentrations (joined by the thick black line in Fig. 4.19), which correspond to particles which do not deposit in the low-velocity slack periods occurring four times a day, are considered in this study to reflect the long-term variation of the wash-load contribution (according to the terminological restrictions of WL as provided above). In this way, a new signal can be generated, corresponding more closely to the suspended-load contribution q_{SL}, namely particles which have the local riverbed as their transient source and sink. Progress in solving the problem raised by Eq. 4.50 is therefore possible if a robust sediment transport model, accounting for the dynamic behavior of the alluvial bed and the associated resuspension process, can be shown to reproduce the q_{SL} component in an acceptable way. An attempt to do this is presented below.

Adaptation of the Bagnold Suspension Model

In view of the complexity of the problem, stationary sediment transport and transport capacity approaches are, at this stage, retained as convenient working hypotheses. Implementation of the model itself is currently performed only locally (zero-D approach) with notably no account for the longitudinal distribution of riverbed deposits. As will be seen, there is ample scope for further model elaboration, as these hypotheses correspond to a gross over-simplification of particle transport processes (Burt et al. 1997; Winterwerp and van Kesteren 2004) occurring in natural, estuarine systems such as the one addressed here.

Based on Bagnold's stream-power concepts (1966), Verbanck (1995) suggested studying the value of $\eta_{SL} C_*$ in the following power balance equation (W m^{-2} of riverbed area):

$$(\rho_s - \rho_l) g w_s C_{SL} R_{Hy} = \rho_l \eta_{SL} C_* u_* (u_*^2 - u_{*c}^2) \tag{4.51}$$

in which R_{Hy} stands for hydraulic radius, w_s effective settling velocity, C_* non-dimensional Chezy coefficient (the one divided by $g^{1/2}$), η_{SL} suspension efficiency, u_* shear velocity, and u_{*c} shear velocity at the onset of motion for sediments forming the channel bed. The left part of Eq. 4.51 is well-known (Bagnold 1966; Yalin 1977) and represents the gravitational power of immersed suspended sediments on their way towards the riverbed at velocity w_s. Without η_{SL}, the right part of Eq. 4.51 is the stream power, calculated as the product of one-dimensional velocity and shear stress in excess of that required to put the deposited particles into motion. The power balance simply expresses that the gravitational power of the transported material uses a certain fraction (η_{SL}) of the available stream power to remain suspended in the water column. This assimilates a river flow to a certain sediment-transport engine, characterized by a given efficiency. Comparatively to previous versions of the suspension model (Verbanck 1996; Ma and Verbanck 2003), Eq. 4.51 also specifies, that under a certain threshold power, the concentration of bed-material particles transported in the water column drops to zero.

In Bagnold's (1966) approach, particles denser than water are maintained suspended in the column through the upward components of the burst cycle, a non-isotropic turbulent process inherent to high-speed flow close to a wall boundary (the riverbed in this case). It is therefore logical to try to relate the sediment transport efficiency to the burst intensity (Leeder 1983; Verbanck 2004b). Resuspension by burst activity implies that the flux of turbulent fluid momentum away from the boundary is exceeding, at least by a small amount, the one returning towards it. With obviously a plane bed in mind, Bagnold examined what are the consequences of these turbulent features developing over a unit area of riverbed. As a result of the net transfer of *upward* momentum, there is an equivalent pressure disturbance created at the boundary, the instantaneous magnitude of which is difficult to quantify. However, averaged over a sufficient number of burst cycles, the overall excess pressure is denoted Δp. Expressed per unit of bed area it has units (N m^{-2}). The suspension efficiency derived by Bagnold actually relies on a model for the prediction of the maximum possible value of Δp (denoted $\Delta p\wedge$ as a reminder of the resuspension effect) as a function of stream power conditions. Making $\Delta p\wedge$ directly proportional to the shear stress distributed over the unit bed area (see Table 4.9) he derived for $\eta_{SL} C_*$ the constant value $\kappa^{1.5}$ (= 0.266). He was satisfied that the choice of this constant value, produced semi-theoretically for a plane bed, reasonably predicted the transport capacity condition for suspended sediments in alluvial rivers. There is thus in this approach no explicit consideration for the bed morphology condition and its consequences in terms of resistance to flow.

Table 4.9. Full magnitude of pressure change created at the boundary by burst activity, $\Delta p\wedge$ (N m^{-2})

Bagnold 1966	$\Delta p\wedge = \kappa \tau_0$	Semi-theoretical (boundary considered as a plane)
This study (in which, by definition, $m \geq 1$)	$\Delta p\wedge = \left(\frac{2\pi}{m}\right)^{10/13} \kappa^2 \tau_0$	Deduced from actual alluvial channels (with bedforms)

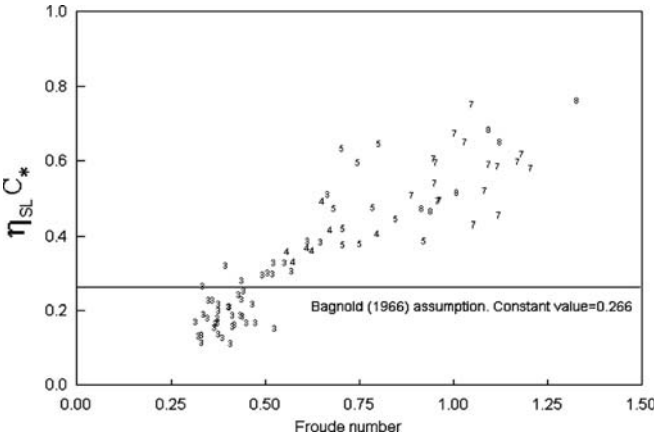

Fig. 4.20.
Questioning the validity of Bagnold's assumption, based on flume runs by Guy et al. 1966 (d_{50} = 0.19 mm, 0.27 mm, 0.28 mm), and Stein 1965 (d_{50} = 0.40 mm). Observed sediment transport rates q_{SL} are used, by application of Eq. 4.51, to deduce the values taken by $\eta_{SL} C_*$ when dune bedforms are progressively washed out and replaced by the bedform configurations typical of the upper alluvial regime

In more recent developments, interpretation of flume and field data performed by Bennett (1973) suggested that considering the product $\eta_{SL} C_*$ as invariant was not a sufficient approach to the problem, given the extended particle-size and stream-power ranges experienced in natural alluvial stream dynamics. Accordingly, Celik and Rodi (1984, 1991) proposed improving the prediction of $\eta_{SL} C_*$ by making it dependent on the value of the relative roughness. The relevance of this criterion for particles as fine as those of interest here was questioned, however, by Westrich and Juraschek (1985) who conducted flume studies of non-depositing flows loaden with quartz particles as fine as 26 µm. By comparing the $\eta_{SL} C_*$ values observed, over erodible and non-erodible boundaries, they were able to demonstrate the significant influence of the separation effect produced by bedform development. A further investigation of the role of the morphological adaptation of the movable bed in controlling the efficiency of suspended sediment transport was recommended (Yalin and Da Silva 2001).

Considering only non-cohesive, single-grain particles under capacity transport in a flume, the value of $\eta_{SL} C_*$ is plotted in Fig. 4.20 as a function of the alluvial regime, reflected both by the ambient Froude number $U/(gD)^{1/2}$ (abscissa) and by the observed bedform configuration phase (datapointer numbered from BF1 to BF8, following the bedform nomenclature suggested by Simons and Richardson 1966).

Figure 4.20 suggests that it is only in a limited alluvial regime range (BF3, corresponding to the fully developed dune configuration) that field sediment transport capacities would be acceptably predicted using Bagnold's assumption. Although Bagnold commented that the $\kappa^{1.5}$ constant would primarily apply to 'higher stages of flow' and upper regimes (bedform BF5 to BF8), this is not substantiated by the general trend depicted in Fig. 4.20. In fair retrospect, it is possible that the fully developed dune configuration, as observed in actual alluvial rivers, has constituted the bulk of experimental evidence examined in the light of Bagnold's suspension model, contributing to its undeniable success among practitioners (Peters 1976). In this study, we retain our confidence in Bagnold's rational leading to the general power balance. However, in Eq. 4.51, we introduce a non-constant value of $\eta_{SL} C_*$, under the form of a dependence with Rossiter modes as recently introduced in alluvial hydraulics studies (Verbanck 2006; Huybrechts and Verbanck 2006).

Inferring Resuspension from Vortex-Generated Wall-Pressure Signals

Rather than skin-friction drag or form-drag, we rely on vortex maintenance to explain how rivers flowing over alluvial bedforms with a characteristic wavelength λ_{BF} (Fig. 4.21) dissipate mean motion energy. The effect of topographic forcing, basically a non-turbulent process, will be addressed below. Shear layer vortices are generated behind the dune crest, where flow separates, and impinge on the back of the next dune at the distance x_R, where streamlines reattach. Experimental evidence collected in large sandbed alluvial channels (Venditti and Bauer 2005; Best 2005) showed that secondary eddies, generated at the point of impingement, could be strong enough to be perceptible at the water surface, displaying characteristic periodicity. Levi (1983a) studied similar oscillatory flow processes with frequency f_{vortex}, that arise when a restrained fluid body, of characteristic length dimension L, interacts with a free flow of mean velocity U. Prediction of the frequency of the periodic perturbations was possible with a Strouhal law of the form:

$$f_{vortex} = \frac{1}{2\pi}\frac{U}{L/m} \tag{4.52}$$

in which $m = 1$ corresponds to the fundamental frequency ($m = 2, 3$, etc. being the higher harmonics, Levi 1983b). The role of control factor m in Eq. 4.52 is the exact counterpart, in aerodynamics, of the dynamical mode number intervening in the Rossiter equation: as soon as it takes an integer value, resonance is active and allows the self-sustained oscillations to be maintained, the most efficient resonance effect taking place at $m = 1$ (Rossiter 1962). Using Eq. 4.52 as a way to predict the periodicity of the vortices in the separation region implies that $m/2\pi$ is the characteristic Strouhal number: a first application of Eq. 4.52 is thus the prediction of the frequency of oscillation. Reversely, spatially periodic structures engendered by the oscillation are controlled by

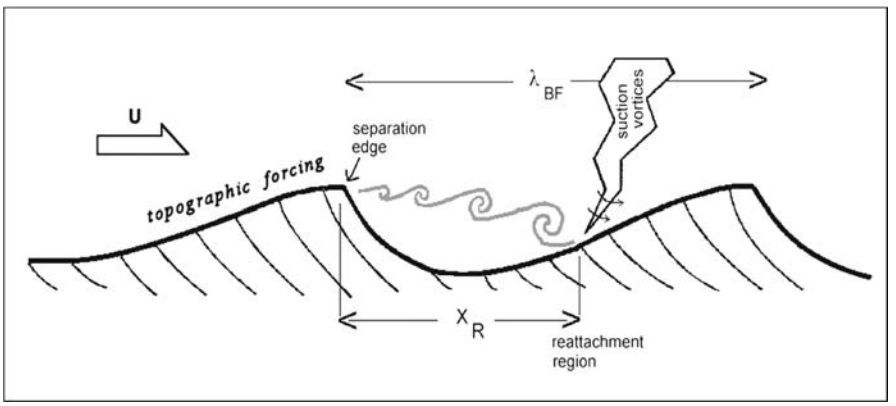

Fig. 4.21. Detached/attached flow model: the movable-bed resistance, predicted as Eq. 4.53, is perceived as the combination of **a** topographically forced attached flow, basically a non-turbulent process, and **b** instabilities in the separated shear layer which originates at the bedform crest (Verbanck 2004b). In this flow configuration, suction vortex dynamics is considered as the main resuspension process

the value of m, allowing m to be placed at the center of a revised bedform typology. In this respect as well, $m = 1$ is to be seen as the condition of the most effective water-transport engine.

On this basis, the attached-detached flow model developed by Verbanck (2004b) provides a way to predict the value of S, the slope of the energy grade line, for a quasi-2-D turbulent open-channel flow over mobile bedforms:

$$S = \left[\frac{\text{gravity forces}}{\text{stationary inertial forces}}\right]^{-5/3}\left[\frac{\text{stationary inertial forces}}{\text{nonstationary inertial forces}}\right]^{-10/3} \tag{4.53}$$

This formulation in two components (based on the Froude number and Strouhal numbers) allows the identification of the modes of energy transfer. In this formulation, bursting activity is undoubtedly reflected by the second term on the right side. It is the one that we want to interpret in light of the pressure change $\Delta p\wedge$ created at the boundary by the periodic vortex impingement at the reattachment point shown in Fig. 4.21, and the possible link with secondary turbulent structures active in resuspending particles. Here again, an analogy can be made with what is known in experimental aerodynamics. Detailed examination of pressure patterns created by turbulent flow along a wall has led Dinkelacker (1982) to conclude that an important part of pressure disturbances can be attributed to a special form of burst activity. With a flow model he showed that 'tornado-like' vortices developing over the wall zone could be responsible for significant momentum transfer across the boundary layer, while explaining the pressure observations at the wall. Turbulent mixing achieved in this way would be very efficient and we see no reason why a similar process and its resuspension consequences should not apply in hydrodynamics (Baud and Hager 2000) and, in the present instance, to the near-bed zone in a river. Accordingly, 'suction-vortices' is the designation retained here to represent the nearly-vertical turbulent structures (Fig. 4.21) which, at their base, literally suck out the particles deposited on the back of the next bedform (Ha and Chough 2003) and then propel turbid clouds upwards. These clouds often take the form of characteristic twirling boils (Gyr and Hoyer 2006), as represented in the sketch above.

When these boils are powerful enough to be observed at the water surface, study of their periodicity (as performed experimentally by, for example, Jackson 1976; Kostaschuk 2000) has shown that it is reasonably described by a Strouhal law prediction. This is the reason why we place the Strouhal number (as occurring in Eq. 4.53) in the center of the resuspension modeling effort. In a flow configuration such as the one illustrated in Fig. 4.21, the topographical forcing repeated from λ_{BF} to λ_{BF} will generate a gravity wave tending to reconstitute a planar, free surface. At the considered disturbance scale, surface tension effects can be neglected. The speed of propagation of the gravity wave is thus simply predicted as (Airy's law):

$$c = \sqrt{\frac{g}{2\pi/\lambda_{BF}}\tanh\frac{2\pi D}{\lambda_{BF}}} \tag{4.54}$$

with D being the total depth and g the acceleration of gravity. The ratio of average stream velocity U to celerity c is called the generalized Froude number (Fr_g). It is this general form which is retained in the logic of Eq. 4.53 (where it actually occurs as Fr_g to

the power 10/3). Equation 4.54 shows that it is only for high values of the ratio λ_{BF}/D that Fr_g converges to the traditional Froude number $U/(gD)^{1/2}$ (the one used, e.g., in Fig. 4.20).

The evidence collected within the Aquaterra project suggests that the pressure change $\Delta p\wedge$ responsible for sediment resuspension actually involves the Strouhal number in a way which presents a striking similarity with Eq. 4.53:

$$\left[\frac{\text{stationary inertial forces}}{\text{nonstationary inertial forces}}\right]^{-10/3} = \left[\frac{\Delta p\wedge}{\kappa^2\tau_o}\right]^{-13/3} \tag{4.55}$$

It is possible that Eq. 4.55, and the value of the exponents (which are retained as such because of the strong standing of Eq. 4.53 so far, Luong and Verbanck 2007) will in the future be further interpreted in the light of turbulent wall-pressure patterns. It is indeed interesting to note that a similar minus ten-third dependency law has been observed to fit reasonably turbulent wall-pressure signatures as expressed in the frequency spectrum form (Black 1966; Hinze 1975).

Equation 4.55 can also be put into the form of Table 4.9, which clarifies how we would now predict the value of $\Delta p\wedge$ (compared with Bagnold's suggestion for a riverbed treated essentially as a plane boundary, with no explicit consideration of bedform influence).

In the special condition of in-phase waves ($m = 1$), the magnitude of $\Delta p\wedge$ reaches a maximum value for a given mean distributed bed stress. The so-called 'antidune standing wave' condition thus constitutes the most efficient bed configuration to produce extreme sediment flux for a given τ_o. This, however, also needs to be appreciated in the light of Eq. 4.53, which implies that, for a given Froude number, $m = 1$ will create the least shear stress at the bed (headloss varying as $m^{10/3}$). The transport capacity formula emerging from this analysis should therefore reflect the dual intervention of the control factor m on particle transport processes, once as an enhancing factor, and once as an inhibition term. This opposition between mixing performance and fluid-flow efficiency is well known in other fluid-mechanics problems, such as turbomixer design and chemical reactor engineering.

The combination of Eq. 4.51 with Eq. 4.55 gives an expression for the volumetric concentration of suspended load (Eq. 4.56). Compared with existing transport capacity approaches (Yalin 1977; Molinas and Wu 2001; Yang 2005 and references therein), this is, to our knowledge, the first sediment transport equation which explicitly takes into account the bedform configuration phase, through the control factor m. It is therefore particularly suited to the interpretation of observations in natural alluvial streams, such as the turbidity records obtained in the Scheldt Estuary in Antwerp.

$$C_{SL} = \kappa^3\left(\frac{2\pi}{m}\right)^{15/13}\frac{u_*S}{\Delta w_s}\left(\frac{\theta-\theta_c}{\theta}\right) \tag{4.56}$$

The prefactor κ^3 is a simple numerical coefficient (0.071) from the data analysis, and the κ^3 notation was retained because it was the same as the square of the $\kappa^{1.5}$ initially suggested – on theoretical grounds – by Bagnold (1966). θ is the non-dimensional shear stress and θ_c the corresponding threshold value from the Shields diagram. Δ stands for the relative excess density. By the mere logic of its derivation, Eq. 4.56 only applies to the suspended-load component. It is not supposed to reflect bed load

q_{BL} (w_s / u_* ratios significantly higher than 3). For volumetric concentrations higher than 1%, concentration modifiers also need to be introduced, notably to account for the influence on the bulk suspension density and for hindering effects on particle settling behavior at very high suspension concentrations (Wan and Wang 1994).

In the follow-up to the discussion on the magnitude of the sediment-transport efficiency, it is noteworthy that suggesting Eq. 4.56 as a transport capacity formula is equivalent to predicting $\eta_{SL} C_*$ as a function of m raised to the power –15/13. This provides a reasonable explanation for the general shape of Fig. 4.20: the grouping $\eta_{SL} C_*$ takes its highest values when ambient Froude number conditions allow m to get sufficiently close to its minimum possible value ($m = 1$, as expression of Rossiter fundamental mode). In the upper alluvial regime, this only occurs in the so-called 'in-phase waves' bedform configuration (Verbanck 2006). This would explain why datapoints in the right part of Fig. 4.20 are systematically associated with the highest sediment-transport efficiency values. River flows over two-dimensional dunes (that we generally associate with the second possible harmonics $m = 2$) would, in this respect, represent significantly less efficient sediment-transport machines. This corroborates field observations collected from natural alluvial streamflows (Toffaleti 1968). A closer, more appropriate, examination of the influence of bedforms of various extent would be possible through the use of generalized Froude number Fr_g, provided that experimental λ_{BF} values are made available as part of the riverflow characterization effort (see Eq. 4.53).

4.4.3 Comparison of the Suspension Model with Field Data

Automated turbidity records have been obtained to characterize Scheldt estuarine waters in Antwerp since 1998. Samples are taken every 30 min, about 1.5 m below the water surface, from a floating landing stage (Sint Anna site). The device is fit with an internal fouling control, guaranteeing good precision even at low SPM values. Absorbance is measured at 660 nm wavelength. Kaolinite standards are used to convert the

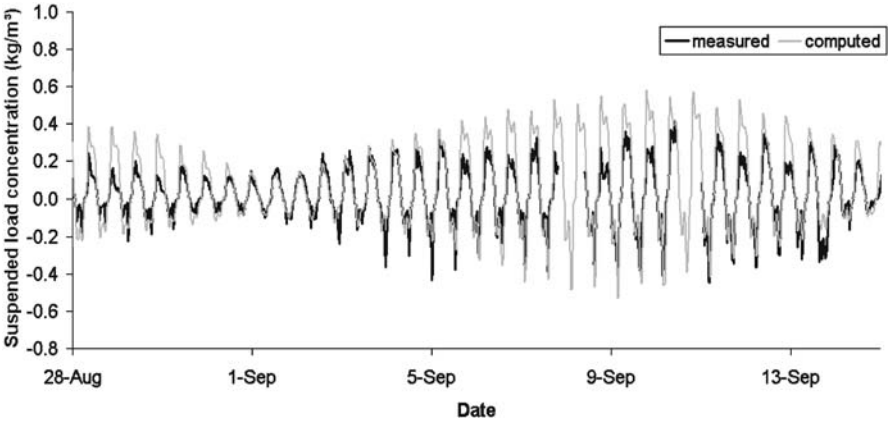

Fig. 4.22. Comparison between experimental suspended solids concentrations (*thick blackline*) and suction-vortex resuspension model output (*light gray line*) for the Scheldt at Antwerp

absorbance signal into SPM concentrations. Figure 4.19 provided an example of a record lasting a few months, illustrating how the 'wash-load' contribution could be taken out of the overall signal. Zooming on a much shorter period, presenting only the suspended-load contribution, Fig. 4.22 shows how local deposited sediments are responsive to stream power increases corresponding to the regular tidal inversions.

Stream velocities in Sint Anna (unfortunately not measured locally) were obtained by a one-dimensional hydrodynamic model proposed by Regnier (1997) for that part of the estuary. The value of the effective settling velocity in the turbulent medium, as occurring in Eq. 4.56, is extracted from the locally observed suspended sediment profiles along the vertical ($w_s = 0.5$ mm s^{-1}) following the method proposed by Verbanck et al. (2002). On this basis, results of the suction-vortex resuspension model, as applied to the eighteen-day continuous sequence, are plotted in Fig. 4.22. To account for the specific estuarine behavior (actually a strong, non-stationary sediment transport system), an invariant time-lag correction of minus 35 min (delay of observed SPM values compared to what they would be in the case of instantaneous response to the hydrodynamic changes) was imposed. To obtain the result shown in Fig. 4.22, the bedform wavelength λ_{BF} (cf. celerity of the gravity wave in generalized Froude number Fr_g, Eq. 4.53) was tuned to 24 m, a value not incompatible with the range of bedform wavelengths (5 m $\leq \lambda_{BF} \leq$ 70 m) usually observed at the site (Francken et al. 2004). Figure 4.22 suggests that, under neap-tide conditions, suspension capacity transport can be observed, fitting very nicely the predictions of the suction-vortex resuspension model. By contrast, this is not true during the largest part of spring tides. It is very likely that, when stream power conditions are the highest, the local source of easily erodible deposits is completely exhausted, exposing old layers characterized by very low erodibility (and very low mud content). If confirmed, this observation in itself could present some operational interest, notably in terms of the sampling strategy to be adopted in further estuarine environmental surveys.

Concluding Remarks

Regarding suspended load predictions, model results proposed so far for the highly dynamical Scheldt sediment system are encouraging, although, surprisingly, they were obtained without special consideration for the cohesive nature of the deposited material. If suspended load can be predicted along the lines suggested in this study, this could mean for the future that the computed q_{SL} for a given river (even a non-tidal one) could be substracted from the experimental SPM record collected during a sufficiently long time. With Eq. 4.50, this would allow the generation of a new, relatively clear q_{WL} experimental signal (no longer obscured by the dynamics of local river deposits). Although obtained in an indirect way, the reconstituted q_{WL} record could serve as a basis for the development of a new generation of wash-load prediction models (irrespective of any terminology arguments about what these WL contributions may be). Assessment and management of non-point sources indeed constitute one of the major challenges of future environmental protection of rivers. The achieved progress is noticeable regarding the control of (municipal and industrial) pollution point-source discharges.

In another respect, consideration of the differences highlighted by the model output between neap- and spring-tide conditions could be exploited from a straightfor-

ward, operational point of view. For further environmental surveys, a model assisted sampling strategy could be considered aiming to optimize, in the temporal and spatial frames, the collection of sediment deposits in highly dynamic estuarine and riverine systems. Sampling and monitoring costs are indeed only justified if there is a sufficient guarantee of sample representativeness. Related concerns are increasing among the EU member states, in their effort to launch the surveillance schemes imposed by the 2000/60 Water Framework Directive.

Acknowledgments

The automated water-quality monitoring station along the Scheldt was operated with the financial help of the Belgian federal state (Management Unit of the Mathematical Model of the North Sea, MUMM). Dr. Pierre Wollast and Mr. Didier Bajura were very instrumental in doing the design and field operation. The first author is much indebted to the discussions shared with Prof. Albrecht Dinkelacker, Max-Planck-Institut für Strömungsforschung, Göttingen. The efficient help of Mrs. Arielle Cornette, operational assistant, is also gratefully acknowledged. Two anonymous reviewers made very constructive comments allowing a previous version of the manuscript to be substantially improved. The study contributes to the AquaTerra Project 'Integrated Modelling of the River-Sediment-Soil-Groundwater System' funded by the European 6th Framework Programme, research priority 1.1.6.3 Global Change and Ecosystems (European Commission, Contract no. 505428-GOCE). It is part of Flux3 'Input/Output Mass Balances in River Basin: Dissolved and Solid Matter Load', a sub-component of the AquaTerra Integrated Project.

References

Bagnold RA (1962) Auto-suspension of transported sediment; Turbidity currents. Proceedings of the Royal Society of London. Series A, Mathematical and Physical Sciences, vol. 265, no. 1322, pp 315–319

Bagnold RA (1966) An approach to the sediment transport problem from general physics, US Geological Survey Professional Paper 422-I, U.S. Department of the Interior

Baud O, Hager WH (2000) Tornado vortices in settling tanks. J Env Eng, 126(2):189–191

Bennett JP (1973) An investigation of the suspended load transport efficiency in the Bagnold equation. IAHR Intl Symp River Mechanics, Bangkok, pp 455–463

Best J (2005) Kinematics, topology and significance of dune-related macroturbulence: some observations from the laboratory and field. Spec Publs Int Ass Sediment 35:41–60

Black TJ (1966) Some practical applications of a new theory of wall turbulence. Proc. Heat Transfer and Fluid Mech. Inst., pp 366–386

ten Brinke WBM (1997) Temporal variability in aggregate size and settling velocity in the Oosterschelde, The Netherlands. In: N Burt, WR Parker, Watts J (eds) Cohesive Sediments. John Wiley & Sons, Chichester

Burt N, Parker WR, Watts J (Eds) (1997) Cohesive Sediments. John Wiley & Sons, Chichester

Cao Z, Carling PA (2002) Mathematical modelling of alluvial rivers: reality and myth. Proc Inst Civil Engrs, Water and Maritime Eng, Part 1 Sept 02 (3), pp 207–219; Part 2 Dec 02 (4), pp 297–307

Celik I, Rodi W (1984) A deposition – entrainment model for suspended sediment transport. Sonderforschungsbereich 210, Universität Karlsruhe

Celik I, Rodi W (1991) Suspended sediment-transport capacity for open channel flows. ASCE J Hydr Eng, 117(2):191–204

Chen MS, Wartel S, VanEck B, Van Maldegem D (2005) Suspended matter in the Scheldt Estuary. Hydrobiologia 540:79–104

Desmit X, Vanderborght J-P, Regnier P, Wollast R (2005) Control of phytoplankton production by physical forcing in a strongly tidal, well-mixed estuary. Biogeosciences 2:205–218

Dinkelacker A (1982) Do tornado-like vortices play a role in turbulent mixing processes? In: Structure of turbulence in heat and mass transfer (Zaric ZP, Editor) Washington DC, Hemisphere Publishing Corp., pp 59–72

Einstein HA (1950) The bed-load function for sediment transportation in open channel flows, USDA Soil Conservation Service (Washington DC), Technical Bulletin no. 1026

Francken FD, Wartel SD, Parker RD, Taverniers ED (2004) Factors influencing subaqueous dunes in the Scheldt Estuary. Geo-Marine Letters 24(1):14–21

Förstner U (2004) Sediment dynamics and pollutant mobility in rivers: An interdisciplinary approach. Lakes and Reservoirs: Research and Management 9:25–40

Guy HP, Simons DB, Richardson EV (1966) Summary of alluvial channel data from flume experiments, 1956-61. USGS Professional Paper 462-I, 96 p

Gyr A, Hoyer K (2006) Sediment transport, a geophysical phenomenon. Fluid Mechanics and its Applications Vol 82, Springer, Dordrecht, 279 p

Ha HK, Chough SK (2003) Intermittent turbulent events over sandy current ripples: a motion-picture analysis of flume experiments. Sedimentary Geology 161(3):295–308

Hinze JO (1975) Turbulence. McGraw-Hill, New York, 2nd ed, 790 p

Huybrechts N, Verbanck MA (2006) Fully-coupled 1D model of mobile-bed alluvial hydraulics with a closure drawn from Rossiter modes resonance concepts. 7th Belgian National Congress on Theoretical and Applied Mechanics, Mons

Kausch H, Michaelis W (eds) (1996) Suspended particulate matter in rivers and estuaries, Advances in Limnology, 47, Stuttgart, 573 p

Kostaschuk R (2000) A field study of turbulence and sediment dynamics over subaqueous dunes with flow separation. Sedimentology 47:519–531

Leeder MR (1983) On the dynamics of sediment suspension by residual Reynolds stresses–Confirmation of Bagnold's theory. Sedimentology 30:485–491

Levi E (1983a) A universal Strouhal law. J Eng Mech, 109(3):718–727

Levi E (1983b) Oscillatory model for wall-bounded turbulence. J Eng Mech 109(3): 728–740

Luong GV, Verbanck MA (2007) Froude number conditions associated with full development of 2D bedforms in flumes. Proc 5th IAHR Symp River, Coastal & Estuarine Morphodynamics, Enschede (NL), acceptedMa TL, Verbanck MA (2003) The minimum slope for preventing accumulation of solids in newly designed sewers. Tribune de l'Eau, no. 624/4:50–59

Molinas A, Wu B (2001) Transport of sediment in large sand-bed rivers. J Hydr Res 39(2):135–146

Owens PN, Batalla RJ, Collins AJ, Gomez B, Hicks DM, Horowitz AJ, Kondolf GM, Marden M, Page MJ, Peacock DH, Petticrew EL, Salomons W, Trustrum NA (2005) Fine grained sediment in river sediments: Environmental significance and Management issues. River Research and Applications 21:693–717

Peters JJ (1976) Sediment transport phenomena in the Zaire River. In: Nihoul JCJ (ed) Bottom turbulence. Elsevier Oceanography series 19, pp 221–236

Regnier P (1997) Long-term fluxes of reactive species in strong tidal estuaries: Model development and application to the Western Scheldt Estuary. Ph.D. thesis, Chemical Oceanography Lab, ULB

Rendon-Herrero O (1974) Estimation of washload produced on certain small watersheds. ASCE J Hyd Eng 100(HY7):835–848

Rossiter JE (1962) The effect of cavities on the buffeting of aircraft. Royal Aircraft Establishment, Tech. Memo. 754:1962

Salomons W, Brils J (eds) (2004) Contaminated sediments in European River Basins. SedNet final summary report, 80 p

Simons DB, Richardson EV (1966) Resistance to flow in alluvial channels. USGS Prof Paper, 422-J

Stein RA (1965) Laboratory studies of total load and apparent bed load. J Geophys Res 70(8):1831–1842

Toffaleti FB (1968) A Procedure for Computation of the Total River Sand Discharge and Detailed Distribution, Bed to Surface, Technical Report no. 5, Committee of Channel Stabilization, Corps of Engineers, U.S. Army, November

Venditti JG, Bauer BO (2005) Turbulent flow over a dune: Green River, Colorado. Earth Surf. Process. Landforms 30:289–304

Verbanck MA (1995) Transferts de la charge particulaire dans l'égout principal de la ville de Bruxelles. Ph.D. thesis, ULB Dept Water Pollution Control, 193 p

Verbanck MA (1996) Assessment of sediment behaviour in a cunette-shaped sewer section. Water Science and Technology 33(9):49–60

Verbanck MA (2004a) Sediment-laden flows over fully-developed bedforms: first and second harmonics in a shallow, pseudo-2D turbulence environment. In: Jirka GH, Uijttewaal WSJ (eds) Shallow Flows. AA Balkema, pp 231–236

Verbanck MA (2004b) Sand transport at high stream power: towards a new generation of 1D river models? Proc 9th International Symposium on River Sedimentation, Yichang, China, Invited paper, pp 307–318

Verbanck MA (2006) How fast can a river flow over alluvium? J Hydraulic Research, in press

Verbanck MA, Laaji A, Niyonzima A (2002) Computing River Suspended Load over Bedforms in the Lower, Transition and Upper Hydraulic Regime. In: Bousmar D, Zech Y (eds) River Flow. Sweet and Zeitlinger, Lisse, pp 625–632

Wang SY (1979) A review of the effective power of sediment suspension in open channel flow – On the criterion of distinguishing bed material load from wash load. Bulletin of Science 24(9):410–413 (in Chinese)

Wan ZH, Wang ZY (1994) Hyperconcentrated flow. IAHR Monograph, AA Balkema, Rotterdam, 289 p

Westrich B, Juraschek M (1985) Flow transport capacity of suspended sediments. XXIst IAHR congress, Melbourne, vol. 3, pp 590–594

Winterwerp JC, van Kesteren WGM (2004) Introduction to the physics of cohesive sediments in the marine environment. Developments in Sedimentology 56, Elsevier, 559 p

Yalin MS (1977) Mechanics of sediment transport, 2nd ed. Pergamon Press, Oxford

Yalin MS, Ferreira Da Silva AM (2001) Fluvial processes. IAHR Monograph, International Association of Hydraulic Engineering and Research, Delft, The Netherlands

Yang SQ (2005) Sediment transport capacity in rivers. J Hydr Res 42(3):131–138

Yen BC (2000) From modeling the Yellow River to river modeling. In: Soong D, Yen BC (eds) First Sino-U.S. Joint Workshop on Sediment Transport and Sediment Induced Disasters, Beijing 15–17 March 1999, Post-Workshop Summary, NSF, 70 p